Rapid Performance Optimization Method of Photoelectrodes

Yannick K. Gaudy and Sophia Haussener[*]

École Polytechnique Fédérale de Lausanne, Institute of Mechanical Engineering, Laboratory of Renewable Energy Science and Engineering, 1015 Lausanne, Switzerland.
[*]E-mail: sophia.haussener@epfl.ch; Tel: +41 21 693 38 78

Abstract

We report the development of a rapid method for the performance optimization of photoelectrodes. The method requires as an input incident photon-to-current efficiency (IPCE) measurements of a material at two or more wavelengths, an estimation of the complex refractive index, the permittivity, the doping concentration, the flatband potential, and the photoelectrode thickness, and estimates in return the diffusion length, the optical loss, the bulk and surface recombination losses, and the space charge region loss. The diffusion optical number, defined as the product of the absorption coefficient and the diffusion length at 500 nm, was used to quantify the performance of photoelectrodes. The method was validated using planar Cu_2O water-splitting photoelectrodes. Subsequently, it was applied to planar water-splitting photoelectrodes made of Cu_2O, Si, Fe_2O_3, $BiVO_4$, $Cu_2V_8O_3$, and $CuFeO_2$, and to nanostructured photoelectrodes made of Fe_2O_3 and $LaTiO_2N$. The projected diffusion optical number of Fe_2O_3 was improved by one order of magnitude when nanostructuring compared to the diffusion optical number of flat Fe_2O_3 photoelectrodes. Thus, a modification of the synthesis or deposition method should be prioritized instead of developing nanostructuring techniques for any photoelectrode with a diffusion optical number two orders of magnitude below the one required to obtain an internal quantum efficiency of 95 %. Using this benchmark, the investigated Si photoelectrode performed well without the need of nanostructuring. Cu_2O and $LaTiO_2N$ photoelectrodes were found to benefit from nanostructuring. In contrast, nanostructuring is not advised for Fe_2O_3, $BiVO_4$, $Cu_2V_8O_3$, and $CuFeO_2$ photoelectrodes, rather their synthesis method should be modified. Approaches for performance improvements by nanostructuring, doping concentration optimization, surface passivation, or by changing the photoelectrode thickness were presented for all investigated photoelectrode materials and nanostructures. We predicted—consistent with previous reporting—that nanostructuring improves the projected diffusion length but also increases the surface recombination losses, which partially counteract the performance improvement, exemplified by the investigated nanostructured Fe_2O_3. The validated tool is well suited to evaluate if nanostructuring can bring a photoelectrode to high performance and/or if the deposition or synthesis methods should be optimized. This tool can also be used for developing new approaches to passivate surfaces and bulk defects, modify doping concentration and investigate their impact on the photoelectrode performance and, more specifically, on the surface and bulk losses. This tool is not restricted to water-splitting reaction but can be applied to any photoelectrochemical reaction.

1. Introduction

Photoelectrochemical (PEC) water-splitting can provide an economically viable solution for large-scale solar fuel production but the photoabsorbers are required to be inexpensive, efficient, and stable for many operating years[1]. Up to now, no photoelectrode can satisfactorily meet all these

requirements and therefore new synthesis methods, nanostructures, or materials need to be discovered[2]. The determination and quantification of a photoelectrode's main limitations such as bulk and surface recombination often require investigations that are time consuming and involve multiple experiments, which are destructive and/or not under realistic operating conditions. Indeed, some photoelectrodes such as hematite photoelectrodes have been investigated for many decades before realizing that even with state-of-the-art nanostructuring methods they are not reaching satisfactory performance. Although the research on such candidates has significantly enhanced the knowledge in the field, we now urgently need rapid and non-destructive techniques to access objectively the performance of actual or emerging photoelectrodes. Such a method allows determining if the synthesis method of the material should be modified or if nanostructuring could be sufficient to reach high performance. The challenges to develop a fast method capable of determining the potential of nanostructuring are manifold. The approach must be capable to separate and quantify losses in the bulk, in the space charge region (SCR), and at the surface. The analysis must be able to extract the diffusion length and the surface recombination loss of the photoelectrodes. Moreover, a criterion that can objectively determine the performance of photoelectrode materials must be established. Finally, the method must be fast, robust and versatile to enable the investigation of various photoelectrode materials and nanostructures. Moreover, the method must be able to quantify the impact of the performance by varying the synthesis methods, by modifying the doping concentration, by passivating the surface, and by nanostructuring, potentially in pristine and at aged conditions. Such a method is currently missing.

Most often, the experimental method to evaluate the potential performance of a photoelectrode is to suppress any surface recombination by using an artificial hole or an electron scavenger. This method is very practical but allows only for a qualitative estimation of the surface and bulk recombination losses. Segev et al.[3] developed a combined experimental-numerical method that provides indications about main material limitations of photoelectrodes. Their method determines the spatial charge collection efficiency and recombination losses of photoelectrodes (exemplified with $Cu_2V_8O_3$ photoanodes) based on optical modeling and incident photon-to-current efficiency (IPCE) measurements[3]. Although their method allows for the determination of the collection length, which accounts for diffusion and drift transport mechanisms, it does not determine the diffusion length, a parameter particularly important for the characterization of photoelectrodes[4] and for quantitative comparison between different photoelectrodes. The determination of the spatial collection efficiency in the work of Segev et al. was originally developed by Tuominen et al.[5] for solar cells. Tuominen et al. used the spectral response of c-Si solar cells to determine the spatial collection efficiency along with the diffusion length and the surface recombination velocity by additionally using the solution of a simplified minority charge carrier conservation equation. More recently, Nakane et al.[6] determined the optical and recombination losses for numerous thin-film photovoltaic devices by fitting the carrier conservation equation of Gärtner[7] to the IPCE. The Gärtner model, initially developed for Schottky junctions, has often been used to determine the diffusion length of photoelectrode materials, i.e. for Fe_2O_3 (ref. 8), $BiVO_4$ (ref. 9), and Cu_2O (ref. 10). This model does neither account for recombination in the SCR nor at the semiconductor-electrolyte interface. Thus, the diffusion length for high permittivity or low doping concentration materials (i.e. conditions resulting in a thick SCR) cannot be determined with this model. Moreover, it cannot separate bulk recombination from surface recombination. We have recently reported on a numerical model solving charge transport and conservation equations by finite volume method (FVM), which has allowed to provided key performing parameters of particle-based (p.-b.) $LaTiO_2N$ photoelectrodes[11]. The use of a 2-dimensional (2D) FVM allowed studying the impact of the morphology on p.-b. photoelectrodes'

performance, which is not accessible with a 1-dimensional (1D) model. However, this model combined bulk and surface lifetimes by the use of a single effective lifetime, which prevented the separation of bulk and surface recombination losses. Moreover, this method required the knowledge of various material parameters (such as electron and hole mobilities and lifetimes) which are unknown for many recently investigated materials and are very challenging and time-consuming to determine.

So far, Fe_2O_3 has been one of the most investigated photoelectrode materials because it is extremely cheap, abundant, stable, and has a suitable bandgap for a well-performing water-splitting tandem device. However, Fe_2O_3 has a low diffusion length that leads to poor efficiency. Early on, optimized meso- and nano-structuring was proposed to reduce the hole path and to overcome the low diffusion length of Fe_2O_3 (ref. 8). Various other approaches to increase the diffusion length of Fe_2O_3 have been explored and included co-catalyst depositions and doping concentration optimization. None of these techniques succeeded in providing highly efficient photoelectrodes.

Here, we introduce a simple and rapid method to calculate the different losses in photoelectrodes and to determine a dimensionless optical and transport parameter, the diffusion optical number. We apply the method to water-splitting photoelectrodes, given by the abundant data available. Our method uses an IPCE model that includes charge carrier conservation equation, continuous states surface recombination at the semiconductor-electrolyte interface[12], SCR recombination, and finite photoelectrode thickness. The IPCE model allows for simple quantification of bulk, SCR, surface and optical losses. The IPCE model is validated by comparing our determined diffusion length of Cu_2O water-splitting photoelectrodes to reported values. We establish a benchmark—based on the diffusion optical number of nanostructured hematite—that sets an objective criterion for the nanostructuring opportunity of a photoelectrode. Our screening method together with the definition of the benchmark is then used to assess nanostructuring opportunity and to suggest performance improvements of numerous photoelectrode materials and nanostructures: planar Cu_2O, Si, Fe_2O_3, Fe_2O_3, $BiVO_4$, $Cu_2V_8O_3$, and $CuFeO_2$, and nanostructured Fe_2O_3 and p.-b. $LaTiO_2N$.

2. Methodology

2.1. Definition of Metrics

The main limitations of a photoelectrode result from internal and surface losses. The internal losses account for bulk and SCR recombination losses. These losses can be described by the diffusion optical number, $\alpha_{500}L$, defined as the product of the absorption coefficient at 500 nm and the diffusion length

$$\alpha_{500}L = \alpha(\lambda = 500 \text{ nm}) \cdot L. \tag{1}$$

$\alpha_{500}L$ is a simple parameter that describes the capability of the photoelectrode to convert light at 500 nm—the wavelength of maximum irradiance of the standard solar spectrum irradiance (AM1.5G)—to exploitable photocurrent. This parameter accounts for the mobility of the charge carrier, the recombination rate of electron/hole pairs, and the absorption coefficient. The diffusion optical number is a practical parameter since it is derived from the approximation of the optimal thickness of a photoelectrode, d^*, given by[13]: $d^* \approx \alpha_{500}^{-1} < W + L$, where W is the SCR thickness. Thus, a high performing photoelectrode must ensure

$$\alpha_{500}(W + L) > 1. \tag{2}$$

If this is not the case, the photoelectrode will not be able to bring enough photoexited charges to the semiconductor-electrolyte interface. Eqn (2) is dependent of the applied potential because W depends on the applied potential (see eqn (11)). When removing W from eqn (2), $\alpha_{500}L$ remains, a factor independent of the applied potential and more convenient for comparison between photoelectrodes. $\alpha_{500}L > 1$ is required for a high performing photoelectrode. The surface losses account for the optical reflection loss and the surface recombination loss. The latter can be described through the ratio of water splitting current and the total current or through the ratio of the surface charge transfer velocity that contributes to the water-splitting reaction, S_T, and the sum of the surface recombination velocity, S_R, and S_T,

$$R_{S,V_\mathrm{IPCE}} = \frac{S_\mathrm{T}}{S_\mathrm{T} + S_\mathrm{R}}. \tag{3}$$

The ratio of currents is determined at a fixed potential at which the IPCE is measured, V_IPCE. This parameter allows evaluating the ratio between surface recombination and charge transfer. $R_{S,V_\mathrm{IPCE}} = 1$ indicates no surface recombination at the semiconductor-electrolyte interface. $R_{S,V_\mathrm{IPCE}} = 0$ implies no photocurrent since charge carriers are fully recombining at the interface.

 The limiting performance of a photoelectrode can be determined if the diffusion optical number and the ratio of currents are identified. The diffusion optical number accounts for all internal losses and the ratio of currents accounts for the surface recombination loss.

 Fe_2O_3 is a good example of a well-studied photoelectrode material having a very low hole diffusion length, in the range of 2-10 nm (ref. 8). Thus, its diffusion optical number is much lower than one, $\alpha_{500}L = 0.03$ (Table 2), which limits the efficiency of this material as a water-splitting photoanode. The nanostructuring of a thin film of the material can be used to overcome minority charge carrier transport limitations, i.e. the high surface area decreases the minority charge carrier transport length. Moreover, nanostructuring often increases the optical scattering providing additional opportunities for absorption to occur and can theoretically overcome a low $\alpha_{500}L$. Nevertheless, this approach has been intensively applied to hematite photoelectrodes over the last decades without leading to a breakthrough performing photoelectrode[14]. Hematite photoelectrodes, as an example, highlight the challenges to overcome the limitations of photoelectrodes with low diffusion optical number. On the other hand, surface recombination limitation such as low reaction kinetic or high surface recombination loss have been successfully overcome by the discovery and incorporation of co-catalysts[15] and passivation layers[16]. Thus, the nanostructuring opportunity of a photoelectrode can be based on the diffusion optical number only.

 To objectively quantify the nanostructuring opportunity of photoelectrodes, we compared the diffusion optical number of the photoelectrode to a second parameter, the diffusion optical number at an internal quantum efficiency (IQE) above 95 %, $\alpha_{500}L_{0.95}$. $\alpha_{500}L_{0.95}$ is defined as the product of the absorption coefficient at 500 nm and the diffusion length, $L_{0.95}$, that provides IQE $\geq$ 95 % at 500 nm, while fixing the surface recombination to zero

$$\alpha_{500}L_{0.95} = \alpha(\lambda = 500 \text{ nm}) \cdot L_{0.95}. \tag{4}$$

$L_{0.95}$ is obtained by solving iteratively IQE(L) $\geq$ 95 % at 500 nm using eqn (6) with S_R=0, for an infinite electrode thickness. The latter ensures that $L_{0.95}$ is not overestimated because of photons that would be transmitted through thin photoelectrodes.

When reviewing the literature, we observed that nanostructuring could only provide an improvement of the diffusion optical number of up to one order of magnitude (see Fe_2O_3 in Figure 6). Thus, it will be very challenging for a photoelectrode with a diffusion optical number more than two orders of magnitude below $\alpha_{500}L_{0.95}$ to perform well when nanostructured. Accordingly, we defined the nanostructuring opportunity factor, f_{nano}, based on the following conditions

$$ f_{nano} = \log_{10}\left(\frac{\alpha_{500}L_{0.95}}{\alpha_{500}L}\right) \begin{cases} > 2 \rightarrow \text{low performance even with nanostructuring} \\ \leq 2 \rightarrow \text{high performance with nanostructuring} \\ < 0 \rightarrow \text{high performance without nanostructuring} \end{cases} . \quad (5)$$

Figure 1 summarizes the method developed to extract the diffusion optical number and the ratio of currents of photoelectrodes. Firstly, we calculate the numerical IPCE, followed by optimizing the fitting of the numerical IPCE to the experimental IPCE through variation of the diffusion length and the surface recombination velocity. The optimization of the IPCE fitting allows for the determination of the diffusion length and the surface recombination velocity and, thus, the diffusion optical number that determines the nanostructuring opportunity of a photoelectrode.

2.2. Numerical Determination of the IPCE

The numerical IPCE of a photoelectrode is calculated by solving the minority charge carrier conservation equation, including i) continuous surface states recombination at the semiconductor-electrolyte interface, ii) recombination in the SCR, and iii) finite photoelectrode thickness. The generation rate in the numerical IPCE model is based on Beer-Lambert law limiting the model to photoabsorption without considering wave interferences or resonant light trapping effects (section 2.6). The full derivation of the following equations—partially based on the work of Wilson[12]—is presented in the supporting information. The IQE of a photoelectrode in function of the photon wavelength (indicated by the subscript λ) is given by

$$ IQE_\lambda = \underbrace{\frac{S_T}{S_T+S_R}}_{\text{surface}} \left[\underbrace{\eta(1-e^{-\alpha_\lambda W})}_{\text{SCR}} + \underbrace{\xi\left(e^{-\alpha_\lambda W}\frac{L}{L+D/S}\frac{\alpha_\lambda L}{\alpha_\lambda L+1}\right)}_{\text{bulk}} \right], \quad (6)$$

where η is a correction term for the SCR recombination, D is the diffusion coefficient, ξ is a correction term accounting for the finite thickness of the photoelectrode, and S is a surface parameter related to the minority charge carrier surface reactions determined by eqn (10). The term $L/(L+D/S)$ can be removed from eqn (6) at a SCR potential larger than 0.23 V (see section 2.4). The diffusion coefficient is related to the mobility of a charge carrier, μ, given by the Einstein relation. η is the ratio between the photocurrent generated in the SCR reaching the semiconductor-electrolyte interface and the recombination current in the SCR, given by

$$ \eta = \frac{i_{SCR}}{i_{rec}+i_{SCR}} = \frac{L^2\phi_{SC}}{W^2 V_{th}+L^2\phi_{SC}}, \quad (7)$$

where V_{th} is the thermal potential given by $V_{th}=k_BT/q$, ϕ_{SC} is the SCR potential given by $\phi_{SC} = V_a - V_{FB}$. V_a and V_{FB} are the applied potential and the flatband potential, respectively. ξ, accounting for the finite photoelectrode thickness, d, is given by

$$\xi = 1 - e^{-\frac{(d-W)(\alpha_\lambda L+1)}{L}}. \tag{8}$$

The surface recombination velocity for continuous surface states is given by integrating the surface states energy levels over the bandgap energy[12]

$$S_R = \int_0^{E_{gap}} \frac{S_{R,0}\cdot e^{-\beta E}}{1+e^{(\phi_{SC}/q-E)/k_BT}}dE, \tag{9}$$

where $S_{R,0}$ is a surface recombination velocity factor and β is a surface states distribution factor. S is given by

$$S = \left[(S_T + S_R)e^{\frac{\phi_{SC}}{V_{th}}} - \frac{1-e^{-\alpha_\lambda W}}{e^{-\alpha_\lambda W}[\alpha_\lambda L/(\alpha_\lambda L+1)]}\frac{D}{L}\frac{\eta}{\xi}\right]\left[1 + \frac{1-e^{-\alpha_\lambda W}}{e^{-\alpha_\lambda W}[\alpha_\lambda L/(\alpha_\lambda L+1)]}\frac{\eta}{\xi}\right]^{-1}. \tag{10}$$

The SCR thickness for a n-type material is given by[13]

$$W = \sqrt{\frac{2\varepsilon_0\varepsilon_r}{qN_D^+}(\phi_{SC} - V_{th})}, \tag{11}$$

where ε_0 and ε_r are the vacuum and the relative permittivity of the material, respectively. N_D^+ is the fully ionized donor doping concentration. Finally, the IPCE or the external quantum efficiency (EQE), is given by adding the reflection loss at the semiconductor-electrolyte interface, R, to the IQE,

$$IPCE_\lambda = EQE_\lambda = IQE_\lambda \cdot (1 - R_\lambda). \tag{12}$$

The reflection loss at the semiconductor-electrolyte interface in function of the wavelength—if not experimentally measured—is given by assuming the imaginary part of the refractive index of the electrolyte being equivalent to water ($k_{water} \ll k_{SC}$) and using the Fresnel equation for normally incident and unpolarized light[17],

$$R_\lambda = \frac{\left[(n(\lambda)-n_{water}(\lambda))^2+k(\lambda)^2\right]}{\left[(n(\lambda)+n_{water}(\lambda))^2+k(\lambda)^2\right]}, \tag{13}$$

where n and k are, respectively, the real and imaginary part of the complex refractive index, $\tilde{n}$, of the semiconductor material.

2.3.   Determination of the Diffusion Optical Number and the Ratio of Currents

The diffusion optical number, $\alpha_{500}L$, and the ratio of currents, $R_{S,V_{IPCE}}$, are calculated from the diffusion length and the surface recombination velocity (eqns (1) and (3)), respectively. The diffusion length and the surface recombination velocity are determined by the IPCE analysis. The IPCE analysis consists of optimizing the fitting of the numerical IPCE given by eqn (12) to an experimental IPCE by varying the diffusion length and the surface recombination velocity (Figure 1). Both parameters were varied with a resolution of 50 points per decade for all our investigated photoelectrodes. This procedure requires that the numerical and the experimental IPCEs are taken at the same applied potential, V_{IPCE}. We investigated most of the photoelectrodes at a single applied potential. This restriction resulted from a lack of experimental IPCE data at different potentials. The numerical method can be applied at any potential without affecting the determination of the diffusion length. However, the surface recombination loss will vary depending on the applied potential (section 2.4). The optimal fitting is determined by maximizing the coefficient of determination, R^2, between the numerical IPCE and the experimental IPCE, given by

$$R^2 = 1 - \frac{\Sigma_i\left(\text{IPCE}_{exp,\lambda_i} - \text{IPCE}_{num,\lambda_i}\right)^2}{\Sigma_i\left(\text{IPCE}_{exp,\lambda_i} - \overline{\text{IPCE}_{exp}}\right)^2}, \tag{14}$$

where the subscript i is the number of wavelengths, λ_i, at which the experimental IPCE, $\text{IPCE}_{exp,\lambda_i}$, was measured. $\text{IPCE}_{num,\lambda_i}$ is the numerical IPCE at the corresponding wavelength, λ_i, and $\overline{\text{IPCE}_{exp}}$ is the average experimental IPCE over all λ_i from the lowest measured wavelength up to the wavelength corresponding to the bandgap of the investigated photoelectrode. In minimum, two different wavelengths are needed and the smaller the smallest wavelength measured the better. If a photoabsorbing material is present on top of the photoelectrode material, the lowest wavelength must be large enough to ensure that the absorption of the top photoabsorbing material is negligible (higher than the bandgap of a semiconductor material).

Since the diffusion length has a spectral effect on the IPCE and, by contrast, the surface recombination velocity is wavelength independent (following the assumtion by Tuominen et al.[5]), we have a unique solution to the IPCE curve fitting problem.
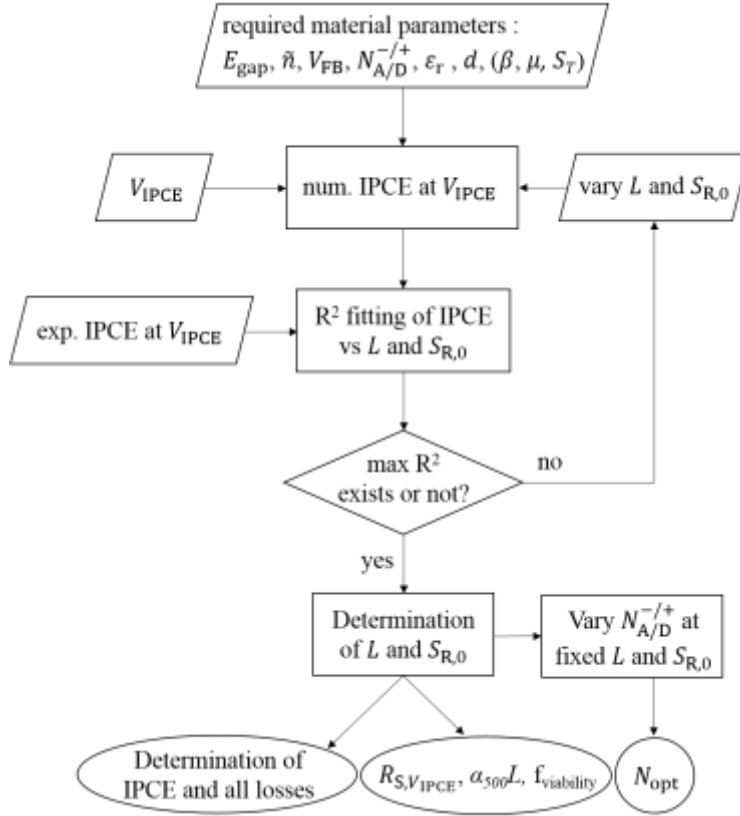
required material parameters :
E_{gap}, $\tilde{n}$, V_{FB}, $N_{A/D}^{-/+}$, ε_r, d, (β, μ, S_T)

V_{IPCE} → num. IPCE at V_{IPCE} ← vary L and $S_{R,0}$

exp. IPCE at V_{IPCE} → R^2 fitting of IPCE vs L and $S_{R,0}$

max R^2 exists or not? no

yes

Determination of L and $S_{R,0}$ → Vary $N_{A/D}^{-/+}$ at fixed L and $S_{R,0}$

Determination of IPCE and all losses

$R_{S,V_{IPCE}}$, $\alpha_{500}L$, $f_{viability}$

N_{opt}

Figure 1. Flowchart of the numerical IPCE analysis used to determine the diffusion length and the surface recombination velocity from which reflection, bulk and surface recombination losses are determined. The ratio of currents, the diffusion optical numbers, the nanostructuring opportunity factor, and the doping concentration that maximize the IPCE are also determined. The inputs are the measured IPCE (at least at two wavelengths, for a given applied potential), the bandgap, E_{gap}, the spectral complex refractive index, $\tilde{n}$, the flatband potential, V_{FB}, the fully ionized acceptor/donor doping concentration, $N_{A/D}^{-/+}$, the permittivity, ε_r, and the electrode thickness, d. The surface state distribution factor, β, the minority charge carrier mobility, μ, and the surface charge transfer coefficient, S_T were assumed (section 2.4).

The impact of the diffusion length and the surface recombination velocity on the IQE is illustrated numerically in Figure 2 for a planar p-Si photoelectrode of 1 mm thickness at $V_{IPCE} = 1$ V$_{RHE}$. Figure 2.a depicts the spectral effect of the diffusion length on the IQE without surface recombination loss. Figure 2.b depicts the wavelength-independence of the surface recombination velocity factor (eqn (9)) on the IQE at an infinite diffusion length. The IPCE remains constant for varying wavelengths up to 1000 nm. The decrease of the absorption coefficient of Si close to 1000 nm (bandgap of 1.12 eV=1107 nm) combined with a finite photoelectrode thickness of 1 mm results in an increase of transmitted photons (not absorbed by the photoelectrode), i.e. a decrease of the IQE above 1000 nm as depicted in Figure 2, even with an infinite diffusion length.
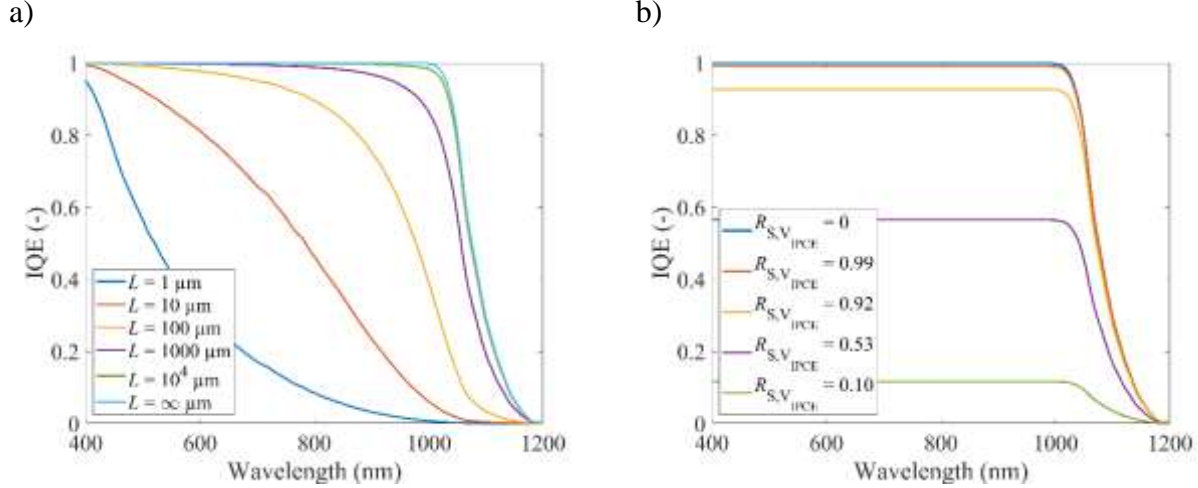
Figure 2. Numerical IQE of a planar p-Si photoelectrode of 1 mm thickness at 1 V_RHE for varying a) diffusion lengths and b) ratios of currents. In a), the surface recombination velocity is fixed to zero and in b) the diffusion length is fixed to infinite and the surface charge transfer to 10^{-2} cm s^{-1}. The ratios of currents at 1 V_RHE in b) were obtained by varying $S_{R,0}$ from 0, 10, 100, 1000, and 10^4 cm s^{-1}.

The internal and surface losses can be easily separated with the numerical IPCE model. The optical reflection loss is determined by eqn (13). The surface recombination loss is determined by the difference between the numerical IPCE with all losses (eqn (12)) and the numerical IPCE without surface recombination loss. The IPCE without surface recombination loss is determined by setting the surface recombination velocity, S_R, in eqns (6) and (10) to zero. The internal loss (bulk and SCR losses) is the IPCE without surface losses (the optical reflection loss and the surface recombination loss). Furthermore, the optimal doping concentration, N_{opt}, can be extracted by finding the doping concentration that maximizes the IPCE at 500 nm (Figure 8).

2.4. Required Material Parameters

As depicted in Figure 1, numerous material parameters, namely the spectral complex refractive index, the bandgap, the flatband potential, the doping concentration, the permittivity, and the thickness of the photoelectrode must be known to determine the diffusion length and the ratio of currents. Even a rough estimate of these parameters still allows for the determination of the diffusion length within the right order of magnitude and thus allows estimating the diffusion optical number and the nanostructuring opportunity factor of the photoelectrode. The impact of the complex refractive index on the determination of the diffusion length was investigated with n-Fe$_2$O$_3$ photoanodes[18]. Although the R^2 of the IPCE fitting was greatly affected by using two different complex refractive indexes—R^2=0.96 using the index of Longtin et al.[19] and R^2=0.57 with Querry[20]— the extracted diffusion length was similar with a value of 8.3 nm with the data of Querry and 9.1 nm with the data of Longtin et al. $R_{S,V_{IPCE}}$ also remained close with $R_{S,V_{IPCE}} = 0.17$ using the index of Querry and 0.23 using the index of Longtin et al. (more details in S2.1). The flatband potential did not significantly impact the determination of the diffusion length of the p-Cu$_2$O photocathode[21]. The diffusion length changed from 1 μm to 1.8 μm using, respectively, a flatband potential of 1.05 V_RHE and 0.73 V_RHE. The $R_{S,V_{IPCE}}$ showed larger sensitivity, i.e. $R_{S,V_{IPCE}}$ varied from 0.97 to 0.84 with respect to a flatband potential of 1.05 V_RHE and 0.73 V_RHE, respectively (more details in S2.2). The doping concentration showed less significance with respect to the diffusion length. A variation of the diffusion length from 1 μm to 5.5 μm was observed when

9

varying the doping concentration between 7.1×10^{13} cm^{-3} to 10^{18} cm^{-3}, respectively. The $R_{S,V_{IPCE}}$ varied from 0.99 to 0.89 with increasing doping concentration from 7.1×10^{13} cm^{-3} to 10^{18} cm^{-3} (more details in S2.3). The impact of the permittivity on the determination of the diffusion length was investigated using the p-Cu$_2$O photocathode[21] at a doping concentration of 7.1×10^{13} cm^{-3}. A variation in the diffusion length from 4.2 µm and 2.4 µm was obtained when the permittivity varied from 1 to 80. The surface recombination loss was reduced from 15 % at a permittivity of 1 to 0.5 % at a permittivity of 80 (more detail in S2.4). The thickness of the photoelectrode did not impact the determination of the diffusion length nor $R_{S,V_{IPCE}}$, as long as the thickness of the photoelectrode was larger than the SCR width (more details in S2.5). The surface state distribution factor, the minority charge carrier mobility, and the surface charge transfer coefficient are inputs parameters with relatively small effect on the results (Figure 1). Indeed, the minority charge carrier mobility could vary between 10^{-3} cm^2 V^{-1} s^{-1} to 10^3 cm^2 V^{-1} s^{-1} without affecting the determination of the diffusion optical number or the ratio of currents as long as the IPCE was measured at a potential region where the SCR potential was above 0.23 V (more details in S2.6). That was the case for all the photoelectrodes investigated in this work and is generally the case since the SCR potential is the main driving force for water-splitting photoelectrodes. Thus, we could remove the term $L/(L+D/S)$ from eqn (6) and ignore the diffusion coefficient and the surface parameter, S, given by eqn (10). The reference minority charge carrier mobility chosen for all photoelectrodes was $\mu=1$ cm^2 V^{-1} s^{-1}. The surface states distribution factor, β, (eqn (9)) influenced the shape of the I-V curves but did not influence the determination of the diffusion length. However, this factor affected the ratio of currents resulting in a surface recombination loss difference of 1 % at 500 nm for $20 \leq \beta \leq 1$ eV^{-1}, using p-Cu$_2$O photocathode as an example (more details in S2.7). $\beta=7$ eV^{-1} was selected for all the photoelectrodes since it best approximated the experimental I-V curve of p-Cu$_2$O photocathode (Figure S3). We determined the value of the ratio of currents (eqn (3)) only and not the surface recombination velocity. The surface recombination velocity could only be obtained when assuming a surface charge transfer velocity of $S_T=10^{-2}$ cm s^{-1}. This value provided $S_{R,0}$ within 1 to 100 cm s^{-1} for all the photoelectrodes investigated in this work, similar to the work of Wilson[12]. We observed that the determination of the diffusion length was not influenced by the choice of the applied potential, V_{IPCE}. Indeed, the diffusion length of the Cu$_3$V$_2$O$_8$ photoanode[3] was found to be 1.7 nm at the two different potentials, 1.21 V$_{RHE}$ and 1.71 V$_{RHE}$. The surface recombination loss decreased from 9.4 % at 1.21 V$_{RHE}$ to 5.1 % at 1.71 V$_{RHE}$, as expected (more details in S2.8).

2.5. Investigated Photoelectrodes

Numerous photoelectrode materials and nanostructures were investigated: a planar p-Cu$_2$O photocathode covered by a Ga$_2$O$_3$/TiO$_2$/RuO$_x$ layer[21], a planar p-Si photocathode covered by a ~80 nm mesoporous hematite layer[22], a planar non-intentionally doped (nid) Fe$_2$O$_3$ and n-Fe$_2$O$_3$ photoanode[18], a planar n-BiVO$_4$ photoanode[23], a planar n-Cu$_3$V$_2$O$_8$ photoanode[3], a planar p-CuFeO$_2$ photocathode[24], nanorods n-Fe$_2$O$_3$ photoelectrodes with and without deposited CoB$_i$ co-catalyst[25], and a p.-b. n-LaTiO$_2$N photoanode[11]. The p.-b. LaTiO$_2$N photoanode was composed of TiO$_2$ inter-particle connections, NiO$_x$/CoO$_x$/Co(OH)$_2$ co-catalysts, and a Ta$_2$O$_5$ passivation layer, as used in our previous work[11]. The generation rate under back illumination (illuminated from the side of the fluorine doped tin oxide glass substrate) followed an exponential decrease along the thickness of the photoelectrode. In contrast, the generation rate under front illumination (illuminated from the LaTiO$_2$N's side) shows a more uniform generation rate, given by the particle density, that follows the exponential absorption behavior[11]. Since our numerical model work for photoelectrodes having a generation rate that follows an exponential decay (as in a homogeneous film), only the IPCE of

10

LaTiO$_2$N photoanodes under back illumination were used to determine the diffusion length and the surface recombination velocity.

Our IPCE measurements of the p.-b. LaTiO$_2$N photoanode is detailed in the supporting information, section S3.1. The IPCE of LaTiO$_2$N at 1.23 V$_{RHE}$ is the average IPCE under back illumination of four fresh photoelectrodes (Figure S5). The complex refractive index of p.-b. LaTiO$_2$N was taken from Gaudy et al.[11] based on reflectance and transmittance measurements. Additionally, we used a complex refractive index calculated by density functional theory (DFT), detailed in the supporting information and Figure S6. The imaginary part of the complex refractive index was reduced according to the average electrode volume fraction of 0.28 within the first 1.42 μm of the active photoelectrode's thickness[11]. The required material parameters for all the photoelectrodes are summarized in Table 1.

Table 1. Material parameters used for the IPCE analysis with references in bracket. n/p-type, is a material doped negatively or positively. $\lambda_{investigate}$ is the investigated wavelength range, R$_{\lambda,m}$, indicates if the reflection loss are experimentally measured ('yes') or numerically calculated according to eqn (13) ('no'). The first value of each parameter is the nominal value, the second or third values are estimated variations.

Material	n/p-type	E_{gap} (eV)	V_{FB} (V$_{RHE}$)	$N_{A/D}^{-/+}$ (cm^{-3})*	ε_r (-)	V_{IPCE} (V$_{RHE}$)	d (nm)	$\tilde{n}$ (ref.)	$\lambda_{investigate}$ (nm)	R$_{\lambda,m}$ (yes/no)
Cu$_2$O	p	2.0[26]	1.05[21,27]** or 0.73[27]	7.1×10^{13}[21]	7.5[27]	0[21]	50 μm[21]	[28]	500-700	no
Si	p	1.12[22]	0.20[29]† or 0.13[22]**	2.5×10^{17} [22,30,31]	11.7[32]	-1[22]	500 μm‡	[33]	600-1000	yes
Fe$_2$O$_3$	n (nid)	2.0[18]	0.34[18]	4.0×10^{18}[18]	32[34]	1.46[18]	25[18]	[19] or [20]	300-700	no
Fe$_2$O$_3$	n	2.0[18]	0.54[18]	2.6×10^{18}[18]	32[34]	1.46[18]	25[18]	[19] or [20]	300-700	no
BiVO$_4$	n	2.5[35]	0.08[23] or 0.1[36]	5×10^{17}[23] 10^{18}-10^{17}	68[37,38]	1[23]†	~200[23]	[39]	320-575	no
Cu$_2$V$_8$O$_3$	n	2.0[40]	~0.5[3]	10^{19}[3] 10^{20}-10^{18}	20[3]*	1.5[3]	283[3]	[3]	320-575	no
CuFeO$_2$	p	1.55[41]	1.01[24]	10^{18}[24]	20[42]*	0.4[24]	290[24]	[24]	350-850	yes
nano-Fe$_2$O$_3$	n	2.0[18]	0.54[18]	2.5×10^{18}[43] 10^{19}-10^{18}	32[34]	1.23[25]	~500	[19]	350-702	no
nano-Fe$_2$O$_3$ -CoB$_i$	n	2.0[18]	0.54[18]	2.5×10^{18}[43] 10^{19}-10^{18}	32[34]	1.23[25]	~500	[19]	350-702	no
LaTiO$_2$N	n	2.1[11]	0.1[11]	7.4×10^{17}[11]	15[11]	1.23$^{\Psi}$	1420[11]	(SI)^e and [11]^e	420-710	yes

*The variations of the doping concentration were estimated based on the frequency dispersion of the Mott-Schottky plot present in the referenced publication. **The flatband potential was calculated using eqn S14 and the difference between the doping concentration of the investigated photoelectrode material and the one of the reference with the published flatband potential value. †The flatband potential was estimated using the method of the inversion of photocurrents[44] to determine the flatband potential. ‡The thickness was assumed to make sure that photons are fully absorbed by the photoelectrode. $^{\Psi}$The IPCE of p.-b. LaTiO$_2$N photoanode was measured in this work under back illumination (Figure S5). ^{e}The absorption coefficient from Gaudy et al.[11] and the one given in the supporting information (SI) were reduced according to the averaged particle density of 0.28 within the first 1.42 μm of the photoelectrode's thickness.

2.6. Model Limitations

The IPCE model does not account for majority carrier charge transport or reaction and therefore any limitation due to the majority charge carriers was not considered. The model is limited to photoelectrodes having a thickness equal or larger than the SCR thickness. If this condition is not fulfilled, as for example for n-Fe$_2$O$_3$ photoelectrodes with a doping concentration of 2.6×10^{18} cm^{-3} (ref. 18) leading to a SCR thickness of 35 nm (eqn (11)), the photoelectrode

thickness was set to a value equal or larger than the SCR thickness. The diffusion length was assumed to be independent of the doping concentration. However, this assumption could be modified by using an empirical relation for the diffusion length as a function of the doping concentration as discussed in section 0. The IPCE must be measured at a potential region where the SCR potential is above 0.23 V so that the charge carrier mobility is not a required parameter (see section S2.6). The model assumes perfectly planar photoelectrodes. With this method, the actual diffusion length is not accessible for a structured photoelectrode and can only be extracted for flat photoelectrodes. However, a projected diffusion length and projected diffusion optical number can be determined for structured photoelectrodes. The projected diffusion length corresponds to the diffusion length obtained by assuming an equivalent perfectly flat photoelectrode providing the same IPCE as for the structured photoelectrode. Thus, the projected diffusion length has to be greater than the actual diffusion length for nanostructured photoelectrodes. If the photoelectrode is perfectly flat, the projected and the actual diffusion length are equivalent and we use the term diffusion length. The generation of electron/hole pairs follows the Beer-Lambert law, thus wave interferences, resonant light trapping, or plasmonic effect were not considered. If these optical effects are significant and induce a generation rate radically different from Beer-Lambert's law, the applicability of the presented method is compromised. Plasmonic effects might be considered by using an effective absorption coefficient if plasmons are introduced homogeneously in the material. Low exitonic binding energy of materials was assumed. Thus, free photogenerated charge carriers are assumed to be related to the absorption coefficient by considering a quantum yield of one. The electric field present in the SCR is assumed to be unperturbed by the photon flux. The doping concentration is constant throughout the entire photoelectrode. The surface recombination velocity and the charge carrier dynamics are wavelength-independent as assumed by Tuominen et al.[5]. All the equations derived to determine the IPCE are at steady-state conditions.

3. Results and Discussions

3.1. Model Validation

The numerical IPCE model was validated by comparing the diffusion length of p-Cu_2O obtained by our IPCE analysis using the experimental IPCE of p-Cu_2O photocathode from Niu et al.[21] with the diffusion length reported by Dimitriadis et al[10]. The experimental IPCE of p-Cu_2O below 500 nm was not considered for the IPCE fitting because of discrepancies in the photoelectrodes with different Cu_2O thicknesses of Niu et al.'s data below 500 nm and to reduce the impact of absorption from the Ga_2O_3/TiO_2/RuO_x layer deposited on Cu_2O (section 2.5). The R^2 of the IPCE fitting was above 0.99 for diffusion lengths varying from 0.9 µm to 2 µm and a ratio of currents of 0.79 to 1 with a maximum R^2 of 0.998 at a diffusion length of 1 µm and a ratio of currents of 0.99 (Figure 3). The determined diffusion length is in agreement with the value of 1 µm found in the work of Dimitriadis et al. for a doping concentration of 9×10^{13} cm^{-3}, close to the doping concentration of 7.1×10^{13} cm^{-3} from Niu et al.

For the maximum IPCE fitting of the p-Cu_2O photocathode, an R^2=0.998 was calculated, indicating a nearly perfect fit between our numerical IPCE and the experimental IPCE of Niu et al. (Figure 4). Hence, our numerical method can also precisely reproduce the experimental IPCE spectra. This is due to the accuracy of our numerical IPCE model but also to the quality of the

complex refractive index data from Malerba et al[28]. Indeed, low quality complex refractive index data can lead to poor IPCE fitting (R^2=0.57) as shown for Fe_2O_3 photoanode (Figure S2).
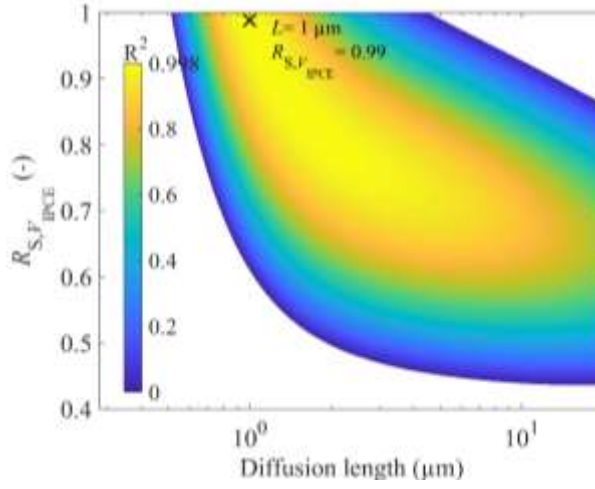

Figure 3. R^2 of the numerical-experimental IPCE fitting at 0 V_{RHE} depending on diffusion length and the ratio of currents for p-Cu_2O photocathode covered by Ga_2O_3/TiO_2/RuO_x (ref. 21). L and $S_{R,0}$ were varied with 50 points per decade from $10^{-0.5}$ to $10^{1.5}$ µm for L and 10^{-2} to 10^3 cm s^{-1} for $S_{R,0}$.

The surface recombination loss represents only 1 % loss in the IPCE at 500 nm (Figure 4), indicating that the combination of a passivation layer and a co-catalyst layer made of Ga_2O_3/TiO_2/RuO_x reduces surface recombination loss ($R_{S,V_{IPCE}}$ increases). Surface recombination loss are usually experimentally determined by comparing the photocurrent obtained in a standard electrolyte to the one in a charge scavenger electrolyte. A charge scavenger can increase the surface charge transfer velocity but does not necessarily completely suppress surface recombination. In contrast, our numerical model can fully separate surface recombination loss from the photocurrent and precisely predict the photocurrent without any surface recombination loss.
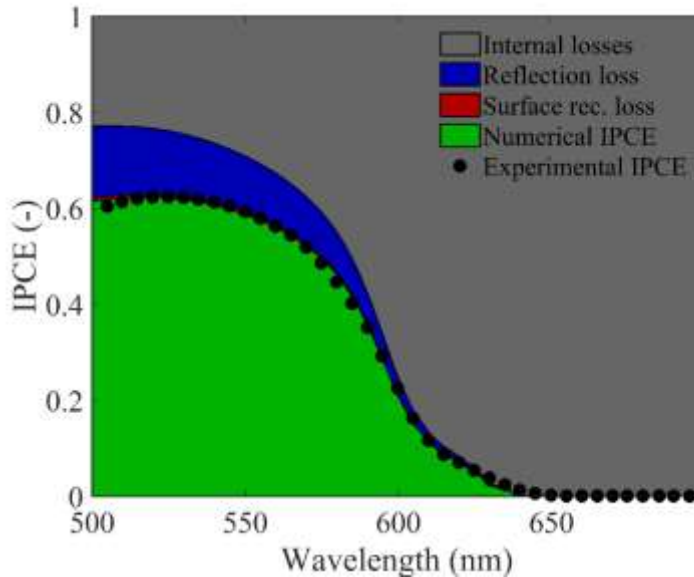
Figure 4. Numerical and experimental IPCE at 0 V_{RHE} for a planar p-Cu_2O photocathode covered by a Ga_2O_3/TiO_2/RuO_x layer with the internal losses (grey), the reflection loss (blue), the surface recombination loss (red), and the numerical IPCE (green). The numerical IPCE was fitted to the experimental IPCE from Niu et al.[21] (black dots).

3.2. Diffusion Lengths and Optical Depths

The diffusion lengths of planar p-Cu_2O, p-Si, nid- and n-Fe_2O_3, and $BiVO_4$ photoelectrodes were determined using our IPCE analysis and were compared to reported values in the literature (Figure 5). All the determined diffusion lengths were within the range of reported values except the one of $CuFeO_2$ with a mismatch of nearly two orders of magnitude. The diffusion length of a planar $Cu_3V_2O_8$ photoelectrode for which, to our knowledge, no diffusion length is currently reported was also determined. The IPCE analysis was additionally applied to determine projected diffusion lengths of nanostructured Fe_2O_3 and p.-b. $LaTiO_2N$ photoanodes (Figure 5). Most of $L_{0.95}$ were within 1-6 µm, except for Si, $BiVO_4$, and $LaTiO_2N$ with values of 15.8 µm, 112 µm, and 3-42.6 µm, respectively (Table 2). Si is an indirect bandgap semiconductor and thus the probability to capture a photon to generate an electron-hole pair is reduced. This low probability results in a poor absorption coefficient and thus must be compensated by a large diffusion length to reach high efficiency. $BiVO_4$ is also an indirect bandgap semiconductor[35] but has a comparatively larger bandgap (2.5 eV or 496 nm compared to 1.12 eV or 1107 nm for Si) that is close to 500 nm at which $L_{0.95}$ is calculated. Therefore, similarly as for Si, the absorption coefficient of $BiVO_4$ at 500 nm is very low and a large diffusion length is also required to reach high efficiency. $L_{0.95}$ of $LaTiO_2N$ varies from 3 to 42.6 µm when using the DFT (section S3.2) or experimental[11] complex refractive index data, respectively. The imaginary part of the experimental complex refractive index, k, of $LaTiO_2N$ was low, which induces a high $L_{0.95}$. We think that the experimental k extracted from p.-b. $LaTiO_2N$ photoelectrodes with a highly complex morphology might be underestimated while the DFT-based k is for a monocrystalline planar $LaTiO_2N$ film, probably providing more realistic k values.

As depicted in Figure 5, Si is the only photoelectrode for which $L_{0.95}$ is smaller than the diffusion length. The diffusion length of Cu_2O is 1-1.8 µm, slightly below the $L_{0.95}$ of 2.4 µm. All the other photoelectrodes have a diffusion length two or three orders of magnitude lower than $L_{0.95}$,

14

except the nanostructured Fe_2O_3-CoB_i and p.-b. $LaTiO_2N$ photoelectrode with a projected diffusion length only one order of magnitude below $L_{0.95}$.

The relatively large variation in the determined diffusion length and $L_{0.95}$ of $LaTiO_2N$ is a result of the different complex refractive index used for the IPCE analysis, one coming from Gaudy et al.[11] and the other one determined by DFT calculations done in this work (Figure S6). The determined projected diffusion length of the p.-b. $LaTiO_2N$ photoelectrode and its variation straddles the determined diffusion length of Gaudy et al.[11] of 280 nm (with a hole lifetime of 0.5 ns and a hole mobility of 61 cm^2 V^{-1} s^{-1}).

The diffusion length of $CuFeO_2$ was found to be 6.3 nm, much below the value of 225 nm determined by time-resolved microwave conductivity measurement (TRMC)[45]. This discrepancy might be due to the fact that TRMC is a technique that cannot discriminate between the mobilities of majority or minority charge carriers while here only the minority charge carrier's diffusion length is determined. Moreover, TRMC determines a local bulk diffusion length while here the diffusion length is not a bulk diffusion length but a projected diffusion length that includes the defects present in the entire photoelectrode. Thus, we believe that TRMC is a technique that potentially overestimates the actual diffusion length. However, a different synthesis technique of $CuFeO_2$, such as physical vapor deposition or chemical vapor deposition, could reduce the defects present in the material and increase the diffusion length.

The calculated projected diffusion length of the nanostructured Fe_2O_3 photoanode covered by CoB_i from Xi et al.[25] was 39.5-119.4 nm, one order of magnitude below $L_{0.95}$ of 3.6 µm (Table 2). The calculated diffusion length of planar Fe_2O_3 was 4.6-9.1 nm, i.e. three orders of magnitude below $L_{0.95}$ (Figure 5).
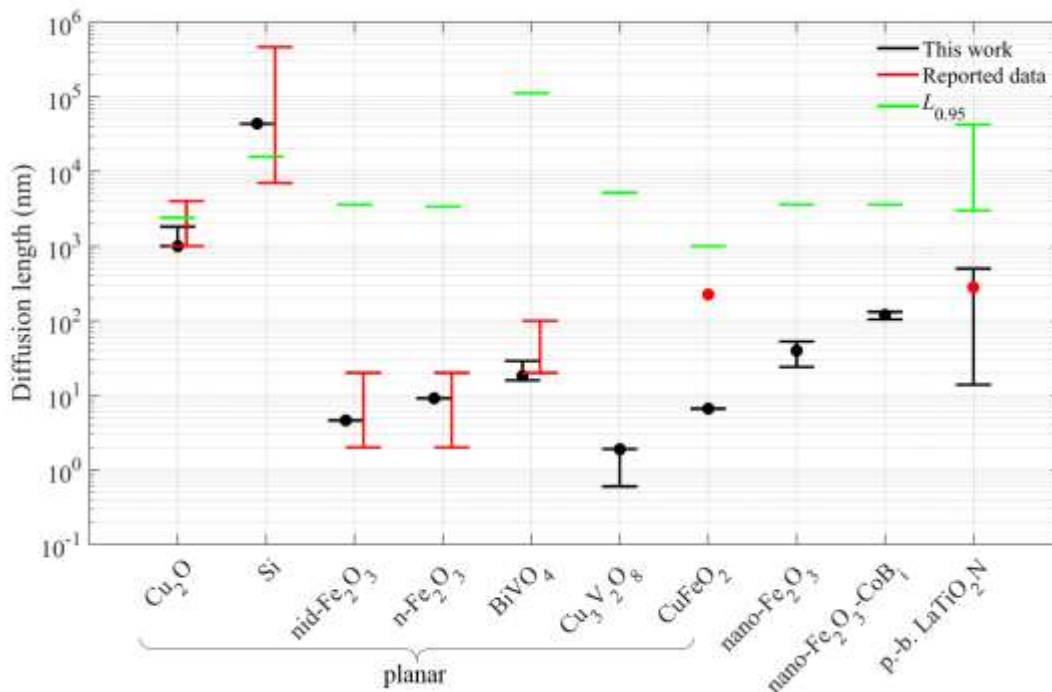

Figure 5. Actual and projected diffusion lengths of all water-splitting photoelectrode materials and nanostructures investigated in this work. The black error bars are the variation in the diffusion length due to variations in the input material parameters (see Table 1) and the black dots are the nominal values. The red error bars are the variation in the diffusion lengths reported in literature. The green lines indicate the diffusion lengths for which the IQE without surface recombination is above 95 % at 500 nm, $L_{0.95}$ (eqn (4)). The diffusion

lengths of Cu_2O reported from literature vary from 1 μm to 4 μm (ref. 10). The calculated diffusion length of Si varies from 7 μm to 467 μm (ref. 31) using a p-Si photoelectrode with a resistivity of 0.01-1 Ω cm (ref. 22) and a doping concentration of 8×10^{18}-1.5×10^{16} cm^{-3} (ref. 30). The diffusion lengths of Fe_2O_3 reported from literature are 2, 3, 4, 10 nm (ref. 8), and 20 nm (ref. 46). The diffusion lengths of $BiVO_4$ reported from literature are 20 nm (ref. 9), 45 nm (ref. 47), 70 nm (ref. 48), and 100 nm (ref. 49). The reported diffusion length of $CuFeO_2$ is 225 nm (ref. 45). The diffusion length of p.-b. $LaTiO_2N$ photoelectrode is 280 nm (ref. 11).

The Si photoelectrode was the only photoelectrode for which the diffusion optical number, $\alpha_{500}L$, was larger than $\alpha_{500}L_{0.95}$, indicating high performance (Figure 6). The Cu_2O photoelectrode is a photoelectrode with $\alpha_{500}L$=3-5 close to $\alpha_{500}L_{0.95}$=7 (Table 2). Thus, Cu_2O photoelectrode is a well performing photoelectrode[21] but can currently not outperform an IQE of 95 % without surface recombination loss at 500 nm (below $\alpha_{500}L_{0.95}$). $\alpha_{500}L$ of Fe_2O_3 photoelectrodes is increased from 0.02-0.04 to 0.187-0.564 by nanostructuring. Thus, nanostructuring improves the projected diffusion length by about two orders of magnitude but only by one order of magnitude for $\alpha_{500}L$, which is not enough to reach $\alpha_{500}L_{0.95}$ (Figure 6).

The diffusion length of p.-b. $LaTiO_2N$ photoanodes is about two orders of magnitude below $\alpha_{500}L_{0.95}$. However, the nanostructure of the investigated p.-b. $LaTiO_2N$ photoanodes[11] is not optimized and a more recent report from Akiyama et al.[50] of p.-b. $LaTiO_2N$ photoanodes with significantly higher specific surface area at reduced electrode thickness shows a photocurrent density at 1.23 V_{RHE}, 7.4 times higher than our photocurrent density, which translates in significantly larger projected diffusion length. Unfortunately, no IPCE data is available in the work of Akiyama et al. and therefore the corresponding diffusion length could not be quantified.
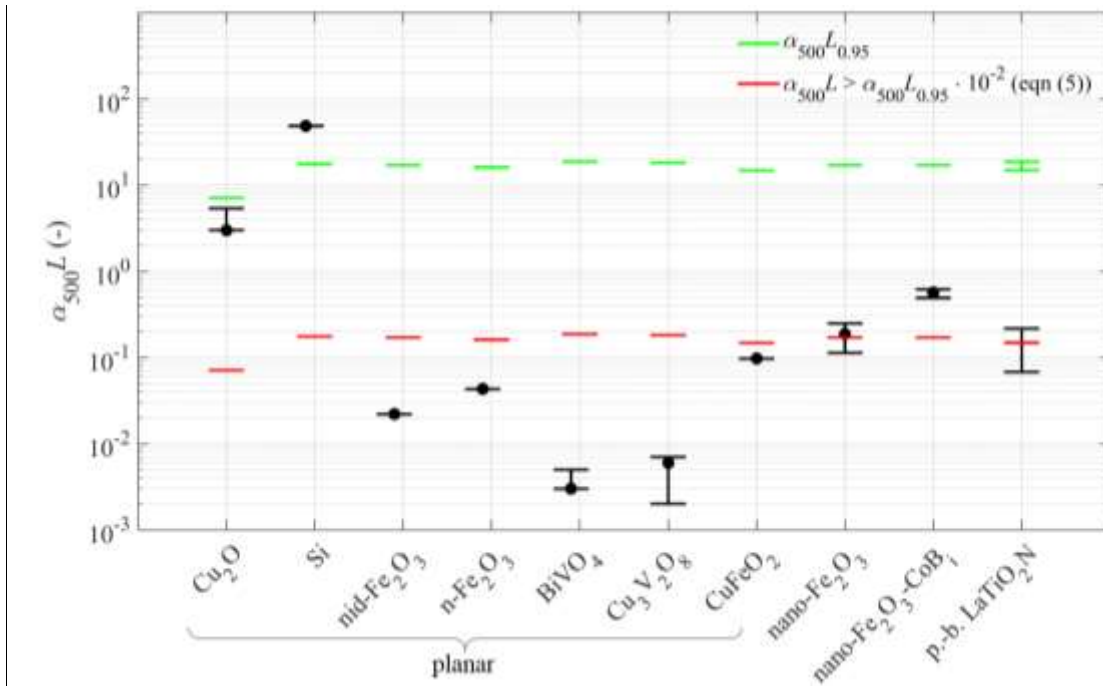

Figure 6. Actual and projected diffusion optical number, $\alpha_{500}L$, of various photoelectrode materials and nanostructures. The green lines indicate the $\alpha L_{0.95}$ for which the IQE without surface recombination is above 95 % at 500 nm (eqn (4)). The red lines indicate the minimum $\alpha_{500}L$ for which a photoelectrode can perform very well when nanostructured (eqn (5)), i.e. an $\alpha_{500}L$ (black lines) below the red line indicates a photoelectrode with low performance even when nanostructured. The black dots are the determined nominal values, the error bars are due to the variations in the input parameters (according to Table 1).

3.3. Pathways to Photoelectrode Improvements

Improvement by Nanostructuring - According to the nanostructuring criterion (eqn (5)), Fe_2O_3, $BiVO_4$, $Cu_3V_2O_8$, and $CuFeO_2$ photoelectrodes are not expected to perform very well, even if nanostructured. Their diffusion optical number, $\alpha_{500}L$, was more than two orders of magnitude below $\alpha_{500}L_{0.95}$ (Table 2). Accordingly, the projected diffusion length of these photoelectrodes should not be improved by nanostructuring but rather by modifying their synthesis method, by reducing the bulk defects and by optimizing the doping concentration. Si and Cu_2O photoelectrodes showed to be good performing candidates since their $\alpha_{500}L$ were in the same order of magnitude as $\alpha_{500}L_{0.95}$. However, Cu_2O photoelectrodes should be nanostructured to achieve an IQE above 95 % at 500 nm. $LaTiO_2N$ is considered potentially good performing since $\alpha_{500}L$ was about two orders of magnitude below $\alpha_{500}L_{0.95}$. Thus, if $\alpha_{500}L$ of particle-based $LaTiO_2N$ photoelectrode could be further improved by nanostructuring, p.-b. $LaTiO_2N$ photoelectrode could become an interesting candidate for high performing water-splitting. Indeed, nanostructuring of p.-b. $LaTiO_2N$ photoelectrodes by increasing the internal nano-pores in contact to the electrolyte using an acidic treatment has been recently achieved and has shown higher performance with a photocurrent density of 8.9 mA cm^{-2} at 1.23 V_{RHE} (ref. 50). We estimate that this increase in the current density translates in an increase of around 50 times the projected diffusion length, i.e. a diffusion length of 694 nm (13.8 nm with our photoelectrodes) calculated with an estimated IPCE of 0.8 at 500 nm for ref. 50, the DFT complex refractive index (see section S3.2) and the material properties of $LaTiO_2N$ (Table 1). Thus, $LaTiO_2N$ photoelectrodes made of mesoscopic particles with optimized, internal nano-pores seem viable photoelectrodes.

Reduction of Surface Losses – In addition to the assessment of the nanostructuring opportunity factor of a photoelectrode, our experimental-numerical method can provide guidance on performance improvements of the photoelectrode. We can calculate the potential improvement by reducing surface recombination and reflection losses. The internal, reflection and surface recombination losses for planar photoelectrodes of Cu_2O, Si, Fe_2O_3, $BiVO_4$, $Cu_3V_2O_8$, and $CuFeO_2$, nanostructured Fe_2O_3, and p.-b. $LaTiO_2N$ photoelectrodes are depicted in Figure 7 (Figure 4 for Cu_2O).

For example, the p-Cu_2O photocathode covered by a $Ga_2O_3/TiO_2/RuO_x$ layer showed only a surface recombination loss of 1 % at 500 nm but a relfection loss of 15 % (Figure 4). Thus, an improvement up to 15 % in the IPCE at 500 nm could be obtained by reducing the reflection loss with an antireflection coating[51]. Nanostructuring the p-Cu_2O photocathode could further improve the performance to an IPCE over 95 % by increasing the projected diffusion length from 1 μm to up to 2.4 μm.

The IPCE of p-Si photocathode covered by a layer of mesoporous hematite[22] was very high, i.e. over 60 % at 600 nm. The reflection loss at the semiconductor-electrolyte interface was taken from the measured reflectance of Li et al.[22] and was minor (1.4 % at 600 nm) according to Figure 7.a. However, the IPCE can be increased up to 26 % at 600 nm by fully suppressing the surface recombination loss (Figure 7.a). The numerical IPCE for this photoelectrode was only investigated for the wavelength range from 600 nm to 1100 nm since the layer of hematite deposited on the Si layer absorbs light until 600 nm, and therefore greatly influences the IPCE below 600 nm.

The IPCE of planar Fe_2O_3 photoanodes could be improved to nearly 30 % at 300 nm when completely suppressing surface recombination loss (Figure 7.c). Nevertheless, the internal losses

related to the short diffusion length of planar Fe_2O_3 1imited the performance to up to an IPCE of 63 % at 300 nm and of 14 % at 500 nm.

The best IPCE fitting of $BiVO_4$ had an R^2 =0.66 only. This poor fitting was observed in Figure 7.d, i.e. the numerical IPCE was 5 % below the experimental IPCE in the wavelength range from 325 nm to 390 nm and 5 % above it in the wavelength range from 400 nm to 470 nm. The poor fitting of the IPCE was a result of the poor refractive index data of $BiVO_4$. Indeed, the complex refractive index giving the best IPCE fit was calculated by DFT of polycrystalline $BiVO_4$ (ref. 39) and not by experimental measurements[35]. Nevertheless, the determined diffusion length of 16-29 nm was within reported data in the literature[9,47–49]. $BiVO_4$ appears to have only a potential IPCE improvement of ~5 % to up to an IPCE of 28 % at 320 nm when fully suppressing surface recombination and reflection losses.

$Cu_2V_3O_8$ and $CuFeO_2$ were both poorly performing photoelectrodes with very limited potential for improvements as planar photoelectrodes, i.e. a maximum IPCE of 16 % at 320 nm for $Cu_2V_3O_8$ and 35 % at 352 nm for $CuFeO_2$ when fully suppressing surface recombination and reflection losses (Figure 7.e and f).

The Fe_2O_3 nanorods photoanode showed greatly reduced internal losses (Figure 7.h) with a projected diffusion length of up to 131 nm. The actual diffusion length of Fe_2O_3 remains within 4.6-9.1 nm (Table 2) while the projected diffusion length of 131 nm for Fe_2O_3 nanorods photoanode is nearly two orders of magnitude (14 times) higher than the actual diffusion length. As mentioned in section 2.6, our method only determines a projected diffusion length for structured photoelectrodes. However, Figure 7.g and Figure 7.h also highlight the challenge raised by nanostructured photoelectrodes, which is the increase of the active surface area and thus an increased surface recombination. Indeed, the surface recombination loss reached 53 % for a nano-Fe_2O_3 photoanode at 350 nm (Figure 7.g) compared to 10 % for nid-Fe_2O_3 at 350 nm (Figure 7.b) or 30 % for n-Fe_2O_3 (Figure 7.c). Nano-Fe_2O_3-CoB_i photoanodes could reach an IPCE of 94 % at 350 nm if the surface recombination and the reflection losses could be fully suppressed. Thus, the deposition of a passivation layer, such as Ga_2O_3 (ref. 21) should be prioritized to increase the efficiency of these nanostructured Fe_2O_3 photoelectrodes. However, even by completely suppressing surface recombination and reflection loss, the IPCE at 500 nm could only reach 45 % because of the low diffusion optical number $\alpha_{500}L$=0.564 (Table 2).

The numerical IPCE of p.-b $LaTiO_2N$ photoanodes did not fit well to the measured IPCE with R^2=0.65 using the index determined in this work by DFT calculation and R^2=0.55 using the complex refractive index of Gaudy et al.[11] (Figure 7.i and j). Reasons for the discrepancy between the numerical and experimental IPCE could lie in inaccurate complex refractive index data of $LaTiO_2N$. As depicted in Figure 7.i and j, the surface recombination loss was independent of the complex refractive index data used (Figure S6 or Gaudy et al.[11]), i.e. there was no surface recombination loss in both cases. Thus, the main internal losses was due to the low projected diffusion length. This result differs from our former conclusion identifying the low surface charge transfer velocity as limiting[11] (interfacial hole transfer velocity). This previous model resolved numerically the electromagnetic wave propagation and the charge transport and conservation in a 2D computational domain representing a typical particle of the film, however neglecting continuous surface state recombination. Here, continuous surface states were considered but the 2D nature of the porous film came into play through the effective properties only, with the minority charge path length limited by our 1D modeling domain. Consequently, the different modeling assumptions favor or punish certain transport mechanism. Most probably, the diffusion length as well as the surface losses are limiting and experiments support this conclusion: increasing the projected diffusion length using nanostructuring and improving the reaction kinetic through the

18

deposition of co-catalysts has shown to improve the performance of p.-b. LaTiO$_2$N photoelectrodes[50].
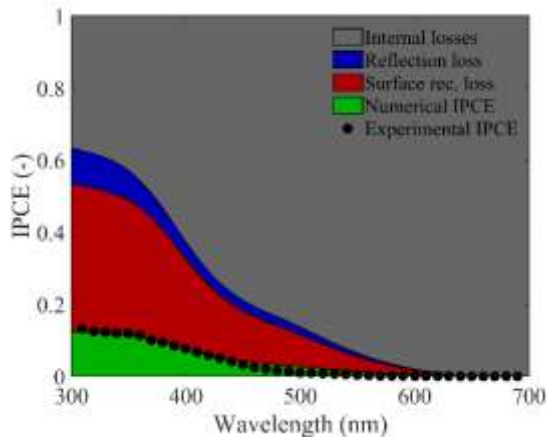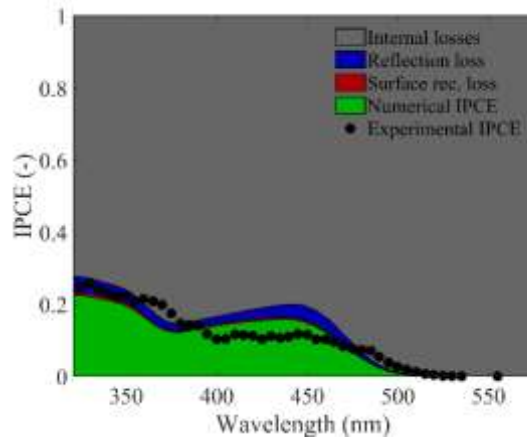
a) p-Si photocathode at -1 V$_{RHE}$, R^2=0.978
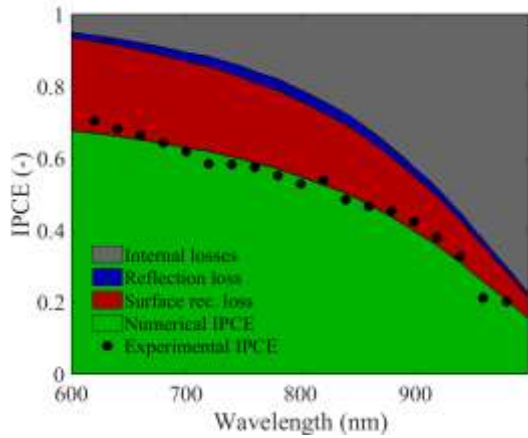
b) nid-Fe$_2$O$_3$ photoanode at 1.46 V$_{RHE}$, R^2=0.843
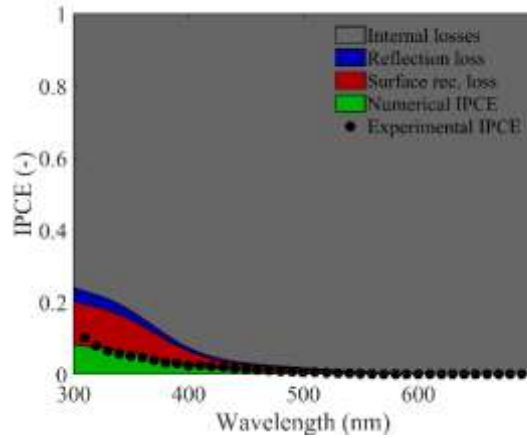
c) n-Fe$_2$O$_3$ photoanode at 1.46 V$_{RHE}$, R^2=0.966

d) n-BiVO$_4$ photoanode at 1 V$_{RHE}$, R^2=0.758

e) n-Cu$_3$V$_2$O$_8$ photoanode at 1.5 V$_{RHE}$, R^2=0.901
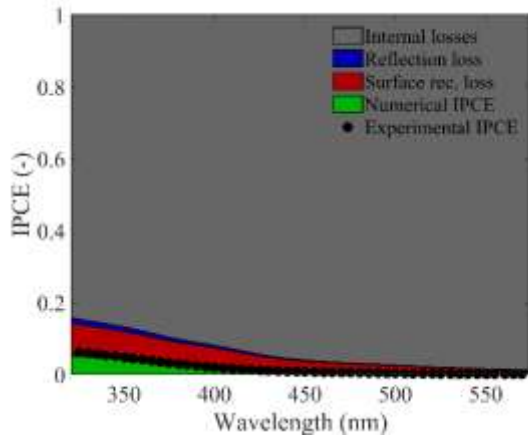
f) p-CuFeO$_2$ photoanode at 0.4 V$_{RHE}$, R^2=0.892
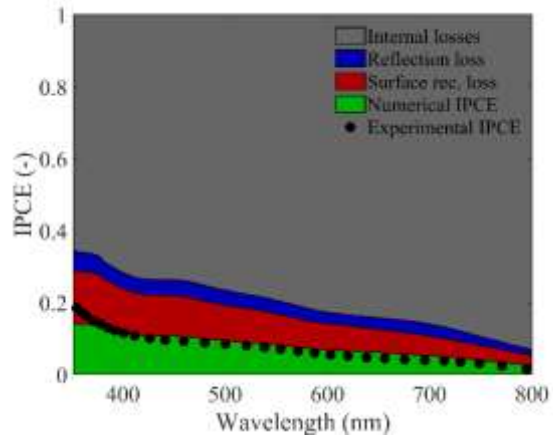
g) nano-Fe$_2$O$_3$ photoanode at 1.23 V$_{RHE}$, R^2=0.991   h) nano-Fe$_2$O$_3$-CoB$_i$ photoanode at 1.23 V$_{RHE}$, R^2=0.992
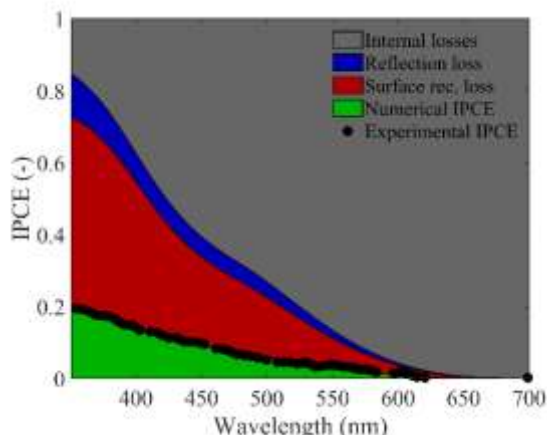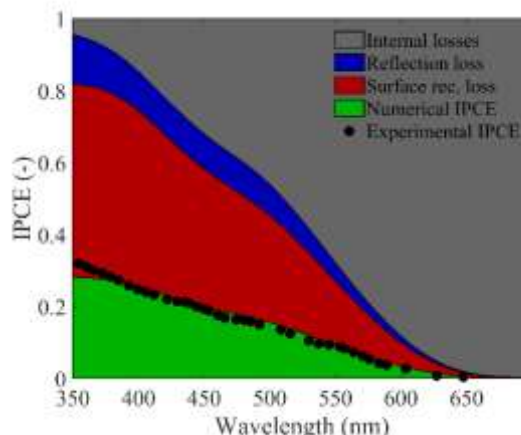
i) p.-b. LaTiO$_2$N photoanode with refractive index from this work (Figure S6) at 1.23 V$_{RHE}$, R^2=0.545   j) p.-b. LaTiO$_2$N photoanode with refractive index at 1.23 V$_{RHE}$, R^2=0.619 from Gaudy et al.[11]
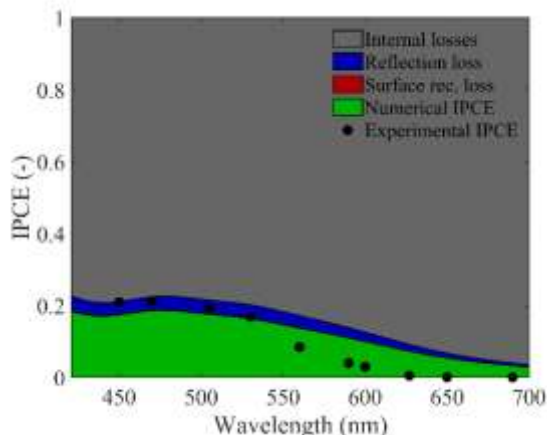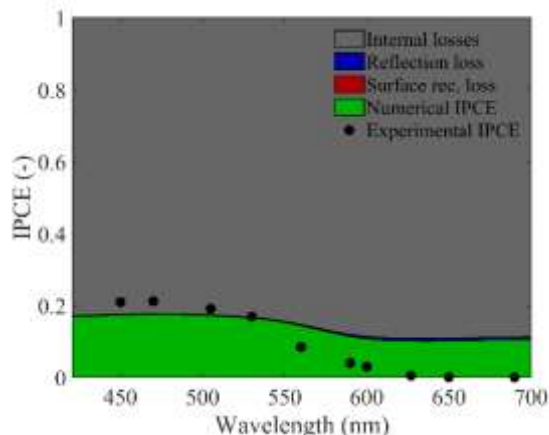
Figure 7. Numerical and experimental IPCE for water splitting a) planar p-Si photocathode covered by a mesoporous layer of hematite[22], b) planar nid-Fe$_2$O$_3$ photoanode[18], c) planar n-Fe$_2$O$_3$ photoanode[18], d) planar n-BiVO$_4$ photoanode[23], e) planar n-Cu$_3$V$_2$O$_8$ photoanode[3], f) planar n-CuFeO$_2$ photoanode[41], g) nanorods n-Fe$_2$O$_3$ photoanode without co-catalyst, h) nanorods n-Fe$_2$O$_3$ photoanode with CoB$_i$ co-catalyst[25], and p.-b. LaTiO$_2$N photoanodes using complex refractive index from i) DFT calculations (Figure S6) and from j) Gaudy et al.[11]and our experimental IPCE measurements (Figure S5). The applied potential of the IPCE, V_{IPCE}, and the R^2 of the IPCE fitting are also indicated.

Optimization of The Photoelectrode's Thickness - The photoelectrode thickness can be optimized for maximal performance. Niu et al.[21] reported that the thickness of their photoelectrode was influencing the IPCE, with the thinnest photoelectrode of 50 μm having the highest efficiency. Since our IPCE model, based only on minority charges, was insensitive to changes in the photoelectrode thickness (down to the SCR width of 3.47 μm, see section S2.5), we can attribute this result to a limitation of the majority charge carrier diffusion length. Thus, our IPCE model can be used to find the minimum thickness for which the IPCE remains unchanged. This minimum thickness will automatically correspond to the smallest, and thus, the optimized thickness for limiting majority carrier diffusion length.

Optimization of The Doping Concentration - An optimal doping concentration—or an optimal SCR width according to eqn (11)—can be obtained by varying the doping concentration without changing the diffusion length nor the ratio of currents. A maximum IPCE at 500 nm and at 0 V_{RHE} was found with a doping concentration of 10^{15} cm^{-3} for the p-Cu$_2$O photocathode of Niu et al.[21] (Figure 8).

The calculated IPCE does not tend to zero with increasing doping concentration (Figure 8) although in reality a semiconductor with high doping concentration becomes degenerated (degeneracy starts at ~10^{20} cm^{-3} for Si) and behaves like a metal, unable to generate any photocurrent and thus the IPCE drops to zero. The numerical IPCE model could account for an IPCE drop to zero for high doping concentration by including the decrease of the diffusion length with increasing doping concentration (see S4 with Si as an example). However, the empirical relation for the diffusion length as a function of the doping concentration is required and is only known for well-established semiconductor materials such as Si, GaN, InP, GaAs, Ge, etc.[52] but not for most photoelectrode materials.
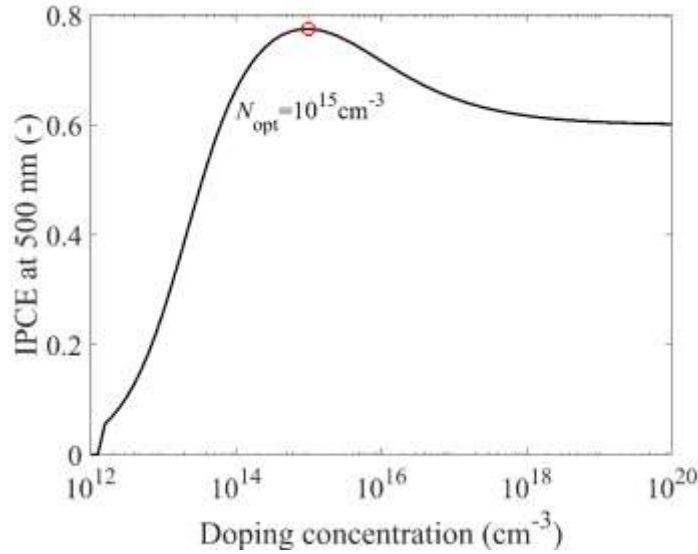

Figure 8. Calculated IPCE at 500 nm as a function of the doping concentration for the p-Cu$_2$O photocathode covered by Ga$_2$O$_3$/TiO$_2$/RuO$_x$ (ref. 21) with a fixed diffusion length of 1 µm (Table 2). A maximum IPCE at 500 nm of 0.78 is obtained at an acceptor doping concentration of 1.0×10^{15} cm^{-3}.

The optimal doping concentrations that maximized the IPCE for all investigated photoelectrodes are presented in Table 2. The predicted optimal doping concentrations are all within experimentally achievable values. However, the synthesis routes of metal oxides do often not offer a precise control of the doping concentration[53]. Table 2 summarizes also the R^2 of the IPCE fitting, the diffusion length, L, the diffusion length that provides an IQE without surface losses higher than 95 %, $L_{0.95}$, the ratio of currents, $R_{S,V_{IPCE}}$, the diffusion optical number, $\alpha_{500}L$, the nanostructuring opportunity factor, f_{nano}, obtained for all the photoelectrodes investigated in this work.

Table 2. Summary of the determined material parameters and factors for all the photoelectrodes investigated in this work. Only nominal values are depicted according to Table 1.

Material	R^2 (-)	L (nm)	$L_{0.95}$ (µm)	$R_{S,V_{IPCE}}$ (-)	$\alpha_{500}L$ (-)	$\alpha_{500}L_{0.95}$ (-)	f_{nano} (-)	N_{opt} (cm^{-3})
p-Cu$_2$O	0.998	1000	2.4	0.99	3.0	7.1	0.4	1.0×10^{15}

p-Si	0.978	43.7×10^3	15.8	0.72	48.5	17.5	-0.4	6.3×10^{13}
nid-Fe$_2$O$_3$	0.843	4.6	3.6	0.18	0.022	17.0	2.9	5.0×10^{18}
n-Fe$_2$O$_3$	0.966	9.1	3.4	0.23	0.043	16.1	2.6	2.5×10^{18}
n-BiVO$_4$	0.657	17.4	112	0.96	0.003	18.6	3.8	6.3×10^{17}
n-Cu$_3$V$_8$O$_3$	0.901	1.9	5.2	0.36	0.007	18.1	3.4	1.6×10^{19}
p-CuFeO$_2$	0.892	6.6	1.0	0.49	0.097	14.8	2.2	2.5×10^{18}
nano-Fe$_2$O$_3$	0.991	39.5	3.6	0.27	0.187	17.0	2	1.6×10^{17}
nano-Fe$_2$O$_3$-CoB$_i$	0.992	119.4	3.6	0.38	0.564	17.0	1.5	4.0×10^{16}
LaTiO$_2$N	0.545	497.9	3.0	1.00	0.217	18.6	1.9	1.3×10^{15}

4.   Conclusion

Decades of research dedicated to the discovery of novel photoelectrode materials have led to a large amount of semiconductor materials with suitable bandgaps for high-performing tandem water-splitting cells. However, none of these materials could provide solutions for efficient, cheap and stable water-splitting photoelectrodes highlighting that the bandgap is not the only criterion for the viability of a photoelectrode. Indeed, charge carrier transport (in the bulk, in the SCR, and across interfaces) has appeared to be as important as the bandgap. Unfortunately, transport properties are much more difficult to evaluate and density functional theory, which is efficient and reasonably accurate in predicting the bandgap of a material, has not yet reached the maturity to accurately predict transport properties. Thus, efforts have been made towards developing rapid techniques to determine the transport properties of photoelectrodes. However, these efforts remain mostly qualitative and have not defined any objective benchmark to evaluate the viability of photoelectrodes or of synthesis method. Here, we have developed a versatile method and coupled it to the nanostructuring opportunity factor in order to objectively investigate if nanostructuring provide a path to reach high performance for a photoelectrode. Furthermore, the method provides an evaluation of the photoelectrode viability by determining if the transport limitation of a photoelectrode can be overcome by nanostructuring and if not, an alternative synthesis method should be developed. Thus, our method could be coupled to experimental high-throughput efforts[54] in order to provide a rapid screening of the viability of novel photoelectrode materials and synthesis methods. The method requires wavelength-dependent IPCE measurements and estimation of the spectral complex refractive index, the bandgap, the flatband potential, the doping concentration, the permittivity and the photoelectrode thickness as inputs and determines in turn the actual or projected diffusion length, the actual or projected diffusion optical number, and the ratio of currents of a photoelectrode. The detailed knowledge of the surface state distribution factor, the minority charge carrier mobility, and the surface charge transfer coefficient is not required since these properties are neither affecting the determination of the diffusion optical number nor the nanostructuring opportunity factor of photoelectrodes. The method was validated with a p-Cu$_2$O photocathode[21] and then used with an objective benchmark to determine the nanostructuring opportunity of water-splitting photoelectrodes. Specifically, a photoelectrode was considered to have a good nanostructuring opportunity if its diffusion optical number was less than two orders of magnitude below the theoretical diffusion optical number ($\alpha_{500}L_{0.95}$), which resulted in an IQE without surface recombination loss above 95 %. This benchmark was established based on the

observed increase in the diffusion optical number of one order of magnitude only of Fe_2O_3 photoanode using state-of-the-art nanostructuring techniques.

We investigated different materials and nanostructures to highlight the versatility of our method. Although only PEC water-splitting photoelectrodes were investigated in this work, there is no restriction to applying our method for any other PEC reactions, including CO_2 reduction. The candidates investigated in this work include planar Cu_2O, Si, Fe_2O_3, $BiVO_4$, $Cu_3V_2O_8$, and $CuFeO_2$ photoelectrodes, and nanostructured Fe_2O_3 and p.-b. $LaTiO_2N$ photoelectrodes. We also presented guidelines for improving the performance of these photoelectrodes by nanostructuring and by evaluating the surface recombination and reflection losses. Furthermore, the doping concentration that maximized the ICPE at 500 nm was calculated for all the photoelectrode materials and nanostructures investigated in this work.

Our IPCE analysis predicted that Fe_2O_3, $BiVO_4$, $CuFeO_2$, and $Cu_3V_2O_8$ have a low nanostructuring opportunity factor ($f_{nano}>2$) due to their low diffusion optical number and thus are difficult to improve with nanostructuring since their internal losses are very high. The nanostructuring opportunity factor of Si was (as the only candidate of all the investigated photoelectrodes) below zero and, thus, could perform without nanostructuring. The use of better catalysts could further improve the performance and at the same time help addressing the stability challenge of Si, a problem still not solved. Since the nanostructuring opportunity factor of Cu_2O was 0.4, we estimate that only a small effort in nanostructuring Cu_2O photocathodes would be required to achieve highly performing photocathodes with an IQE above 95 % at 500 nm. Moreover, a small increase in the doping concentration of up to 10^{15} cm^{-3} could theoretically increase the IPCE at 500 nm by 15 % (from 62.3 % to 77.5 %). P.-b. $LaTiO_2N$ photoanodes could potentially have a high performance as the projected diffusion optical number of the nanostructured p.-b. $LaTiO_2N$ photoelectrode investigated here lied at the limit of our nanostructuring opportunity factor benchmark. Indeed, a report in literature[50] indicates that improved nanostructures of p.-b. photoelectrode have the potential for further improvements in the diffusion length. A similar approach for nanostructured Fe_2O_3 photoelectrodes might be interesting to undertake as these photoelectrodes lied also at the limit of our nanostructuring opportunity factor benchmark. However, since we observed that nanostructuring also increased the surface recombination loss, the deposition of a surface passivation layer or a co-catalyst to suppress surface recombination should be conjointly considered.

The durability of photoelectrodes has not been considered in this work although it is a key factor for cost-effective and industrial scale hydrogen production[55]. Nevertheless, our method could be used in combination with IPCE measurements at different operating times (for example *in-operando*) to evaluate the chronological change (i.e. increase) in surface recombination, internal or reflection losses. The ability to capture the chronological increase of each loss could greatly enhance the understanding of degradation phenomena and their effects on photoelectrode properties. Moreover, the durability could be quantified and used as an additional criterion for the performance of photoelectrodes.

Finally, the ability of our method to provide an estimation of the diffusion length in the right order of magnitude, even if some required material parameters are not precisely known or even unknown, gives an indication that our method can be used as a rapid and facile tool to quickly estimate the viability and the nanostructuring opportunity factor of new photoelectrodes. A user-friendly executable of the developed method is available in the supporting files and on our laboratory webpage[56], software POPe[57].

Author Information

Corresponding Author
Email: sophia.haussener@epfl.ch.

Notes
There are no conflicts to declare.

Supporting Information

Development of the internal quantum efficiency equation. Sensitivity analysis of the complex refractive index, the flatband potential, the doping concentration, the relative permittivity, the photoelectrode thickness, the minority charge carrier mobility, the surface states distribution factor, and the applied potential of the IPCE measurements. IPCE measurements of particle-based $LaTiO_2N$ photoelectrodes and complex refractive index of $LaTiO_2N$ by DFT calculations. IPCE at 500 nm as a function of doping concentration for Si photoelectrode.

Acknowledgments

References

(1)   Pinaud, B. a.; Benck, J. D.; Seitz, L. C.; Forman, A. J.; Chen, Z.; Deutsch, T. G.; James, B. D.; Baum, K. N.; Baum, G. N.; Ardo, S.; et al. Technical and Economic Feasibility of Centralized Facilities for Solar Hydrogen Production via Photocatalysis and Photoelectrochemistry. *Energy Environ. Sci.* **2013**, *6* (7), 1983.

(2)   Jiang, C.; Moniz, S. J. A.; Wang, A.; Zhang, T.; Tang, J. Photoelectrochemical Devices for Solar Water Splitting-Materials and Challenges. *Chem. Soc. Rev.* **2017**, *46* (15), 4645–4660.

(3)   Segev, G.; Jiang, C.; Eichhorn, J.; Toma, F. M.; Cooper, J. K.; Sharp, I. D. Quantification of the Loss Mechanisms in Emerging Water Splitting Photoanodes through Empirical Extraction of the Spatial Charge Collection Efficien. *Energy Environ. Sci.* **2018**, *11*, 904–913.

(4)   Hodes, G.; Kamat, P. V. Understanding the Implication of Carrier Diffusion Length in Photovoltaic Cells. *J. Phys. Chem. Lett.* **2015**, *6* (20), 4090–4092.

(5)   Tuominen, E.; Acerbis, M.; Hovinen, A.; Siirtola, T.; Sinkkonen, J. A Method Extracting Solar Cell Parameters from Spectral Response by Inverse Laplace Transform. *Phys. Scr.* **1997**, *T69* (T69), 306–309.

(6)   Nakane, A.; Tampo, H.; Tamakoshi, M.; Fujimoto, S.; Kim, K. M.; Kim, S.; Shibata, H.; Niki, S.; Fujiwara, H. Quantitative Determination of Optical and Recombination Losses in Thin-Film Photovoltaic Devices Based on External Quantum Efficiency Analysis. *J. Appl. Phys.* **2016**, *120* (6).

(7)   Gärtner, W. W. Depletion-Layer Photoeffects in Semiconductors. *Phys. Rev.* **1959**, *116* (1), 84–87.

(8)   Kennedy, J. H.; Frese, K. W. Photooxidation of Water at α-Fe2O3 Electrodes. *J. Electrochem. Soc.* **1978**, *125* (5), 709–714.

(9)   Zhao, X.; Luo, W.; Feng, J.; Li, M.; Li, Z.; Yu, T.; Zou, Z. Quantitative Analysis and Visualized Evidence for High Charge Separation Efficiency in a Solid-Liquid Bulk Heterojunction. *Adv. Energy Mater.* **2014**, *4* (9), 1301785.

(10)   Dimitriadis, C. A.; Papadimitriou, L.; Economou, N. A. Resistivity Dependence of the Minority Carrier Diffusion Length in Single Crystals of Cu20. *J. Mater. Sci. Lett.* **1983**, *2*, 691–693.

(11)   Gaudy, Y. K.; Dilger, S.; Landsmann, S.; Aschauer, U.; Pokrant, S.; Haussener, S. Determination and Optimization of Material Parameters of Particle-Based LaTiO2N Photoelectrodes. *J. Mater. Chem. A* **2018**, *6* (36), 17337–17352.

(12)   Wilson, R. H. A Model for the Current-voltage Curve of Photoexcited Semiconductor Electrodes. *J. Appl. Phys.* **1977**, *48* (10), 4292–4297.

(13)   van de Krol, R.; Grätzel, M. *Photoelectrochemical Hydrogen Production*; van de Krol, R., Grätzel, M., Eds.; Electronic Materials: Science & Technology; Springer: Boston, 2012.

(14)   Wheeler, D. A.; Wang, G.; Ling, Y.; Li, Y.; Zhang, J. Z. Nanostructured Hematite: Synthesis, Characterization, Charge Carrier Dynamics, and Photoelectrochemical Properties. *Energy Environ. Sci.* **2012**, *5* (5), 6682.

(15)   McCrory, C. C. L.; Jung, S.; Ferrer, I. M.; Chatman, S.; Peters, J. C.; Jaramillo, T. F. Benchmarking HER and OER Electrocatalysts for Solar Water Splitting Devices. *J. Am. Chem. Soc.* **2015**, 150210114104003.

(16)   Liu, R.; Zheng, Z.; Spurgeon, J.; Yang, X. Enhanced Photoelectrochemical Water-Splitting Performance of Semiconductors by Surface Passivation Layers. *Energy Environ. Sci.* **2014**, *7* (8), 2504–2517.

(17)   Siegel, R.; Howell, J. *Thermal Radiation Heat Transfer*, 4th ed.; Bedford, R. H., Ed.; Taylor & Francis: New York, 2002.

(18)   Yan, D.; Tao, J.; Kisslinger, K.; Cen, J.; Wu, Q.; Orlov, A.; Liu, M. The Role of the Domain Size and Titanium Dopant in Nanocrystalline Hematite Thin Films for Water Photolysis. *Nanoscale* **2015**, *7* (44), 18515–18523.

(19)   Longtin, D. R.; Shettle, E. P.; Hummel, J. R.; Pryce, J. D. *Wind Dependent Desert Aerosol Model: Radiative Properties*; 1988.

(20)   Querry, M. R. *Optical Constants*; 1985.

(21)   Niu, W.; Moehl, T.; Cui, W.; Wick-Joliat, R.; Zhu, L.; Tilley, S. D. Extended Light Harvesting with Dual Cu2O-Based Photocathodes for High Efficiency Water Splitting. *Adv. Energy Mater.* **2018**, *8* (10), 1702323.

(22)   Li, S.; Zhang, P.; Xie, X.; Song, X.; Liu, J.; Zhao, L.; Chen, H.; Gao, L. Enhanced Photoelectrochemical Performance of Planar P-Silicon by APCVD Deposition of Surface Mesoporous Hematite Coating. *Appl. Catal. B Environ.* **2017**, *200*, 372–377.

(23)   Li, M.; Zhao, L.; Guo, L. Preparation and Photoelectrochemical Study of BiVO4 Thin Films Deposited by Ultrasonic Spray Pyrolysis. *Int. J. Hydrogen Energy* **2010**, *35* (13), 7127–7133.

(24)   Prévot, M. S.; Guijarro, N.; Sivula, K. Enhancing the Performance of a Robust Sol-Gel-Processed p-Type Delafossite CuFeO2 Photocathode for Solar Water Reduction. *ChemSusChem* **2015**, *8* (8), 1359–1367.

(25)   Xi, L.; Schwanke, C.; Zhou, D.; Drevon, D.; van de Krol, R.; Lange, K. M. In Situ XAS Study of CoBi Modified Hematite Photoanodes. *Dalt. Trans.* **2017**, *46*, 15719–15726.

(26)   Xiang, C.; Kimball, G. M.; Grimm, R. L.; Brunschwig, B. S.; Atwater, H. A.; Lewis, N. S.

820 MV Open-Circuit Voltages from Cu2O/CH3CN Junctions. *Energy Environ. Sci.* **2011**, *4* (4), 1311.

(27) Luo, J.; Steier, L.; Son, M. K.; Schreier, M.; Mayer, M. T.; Grätzel, M. Cu2O Nanowire Photocathodes for Efficient and Durable Solar Water Splitting. *Nano Lett.* **2016**, *16* (3), 1848–1857.

(28) Malerba, C.; Biccari, F.; Ricardo, C. L. A.; D'Incau, M.; Scardi, P.; Mittiga, A. Absorption Coefficient of Bulk and Thin Film Cu2O. *Sol. Energy Mater. Sol. Cells* **2011**, *95*, 2848–2854.

(29) Hou, Y.; Abrams, B. L.; Vesborg, P. C. K.; Björketun, M. E.; Herbst, K.; Bech, L.; Setti, A. M.; Damsgaard, C. D.; Pedersen, T.; Hansen, O.; et al. Bioinspired Molecular Co-Catalysts Bonded to a Silicon Photocathode for Solar Hydrogen Evolution. *Nat. Mater.* **2011**, *10* (6), 434–438.

(30) Zeghbroeck, B. Van. *Principles of Semiconductor Devices*; University of Colorado, 2002.

(31) Tyagi, M. S.; Van Overstraeten, R. Minority Carrier Recombination in Heavily Doped Silicon. *Solid-State Electron.* **1983**, *26* (6), 577–597.

(32) *Handbook Series on Semicondoor Parameters*; Levinshtein, M., Rumyantsev, S., Shur, M., Eds.; World Scientific: Singapore, 1996.

(33) Green, M. A. Self-Consistent Optical Parameters of Intrinsic Silicon at 300 K Including Temperature Coefficients. *Sol. Energy Mater. Sol. Cells* **2008**, *92* (11), 1305–1310.

(34) Klahr, B.; Gimenez, S.; Fabregat-Santiago, F.; Hamann, T.; Bisquert, J. Water Oxidation at Hematite Photoelectrodes : The Role of Surface States. *J. Am. Chem. Soc.* **2012**, *134* (9), 4294–4302.

(35) Cooper, J. K.; Gul, S.; Toma, F. M.; Chen, L.; Liu, Y. S.; Guo, J.; Ager, J. W.; Yano, J.; Sharp, I. D. Indirect Bandgap and Optical Properties of Monoclinic Bismuth Vanadate. *J. Phys. Chem. C* **2015**, *119* (6), 2969–2974.

(36) Ma, Y.; Pendlebury, S. R.; Reynal, A.; le Formal, F.; Durrant, J. R. Dynamics of Photogenerated Holes in Undoped BiVO4 Photoanodes for Solar Water Oxidation. *Chem. Sci.* **2014**, *5* (8), 2964.

(37) Valant, M.; Suvorov, D. Chemical Compatibility between Silver Electrodes and Low-Firing Binary-Oxide Compounds: Conceptual Study. *J. Am. Ceram. Soc.* **2000**, *83* (188846), 2721–2729.

(38) Wee, S.-H.; Kim, D.-W.; Yoo, S.-I. Microwave Dielectric Properties of Low-Fired ZnNb2O6 Ceramics with BiVO4 Addition. *J. Am. Ceram. Soc.* **2004**, *40* (87), 871–874 (2004).

(39) Zhao, Z.; Li, Z.; Zou, Z. Electronic Structure and Optical Properties of Monoclinic Clinobisvanite BiVO4. *Phys. Chem. Chem. Phys.* **2011**, *13* (10), 4746.

(40) Seabold, J. A.; Neale, N. R. All First Row Transition Metal Oxide Photoanode for Water Splitting Based on Cu3V2O8. *Chem. Mater.* **2015**, *27* (3), 1005–1013.

(41) Read, C. G.; Park, Y.; Choi, K.-S. Electrochemical Synthesis of P-Type CuFeO2 Electrodes for Use in a Photoelectrochemical Cell. *J. Phys. Chem. Lett.* **2012**, *3* (14), 1872–1876.

(42) Kimura, T.; Lashley, J. C.; Ramirez, A. P. Inversion-Symmetry Breaking in the Noncollinear Magnetic Phase of the Triangular-Lattice Antiferromagnet CuFeO2. *Phys. Rev. B - Condens. Matter Mater. Phys.* **2006**, *73* (22), 1–4.

(43) Iandolo, B.; Zhang, H.; Wickman, B.; Zorić, I.; Conibeer, G.; Hellman, A. Correlating Flat Band and Onset Potentials for Solar Water Splitting on Model Hematite Photoanodes. *RSC Adv.* **2015**, *5* (75), 61021–61030.

(44) Wilhelm, S. M.; Yun, K. S.; Ballenger, L. W.; Hackerman, N. Semiconductor Properties of

Iron Oxide Electrodes. *J. Electrochem. Soc.* **1979**, *126* (3), 419–424.

(45) Prévot, M. S.; Jeanbourquin, X. A.; Bourée, W. S.; Abdi, F.; Friedrich, D.; van de Krol, R.; Guijarro, N.; Le Formal, F.; Sivula, K. Evaluating Charge Carrier Transport and Surface States in CuFeO2 Photocathodes. *Chem. Mater.* **2017**, *29* (11), 4952–4962.

(46) Dare-Edwards, M. P.; Goodenough, J. B.; Hamnett, A.; Trevellick, P. R. Electrochemistry and Photoelectrochemistry of Iron(III) Oxide. *J. Chem. Soc. Trans. I* **1983**, *79* (1), 2027–2041.

(47) Antony, R. P.; Bassi, P. S.; Abdi, F. F.; Chiam, S. Y.; Ren, Y.; Barber, J.; Loo, J. S. C.; Wong, L. H. Electrospun Mo-BiVO4for Efficient Photoelectrochemical Water Oxidation: Direct Evidence of Improved Hole Diffusion Length and Charge Separation. *Electrochim. Acta* **2016**, *211*, 173–182.

(48) Abdi, F. F.; Savenije, T. J.; May, M. M.; Dam, B.; Krol, R. Van De. The Origin of Slow Carrier Transport in BiVO4 Thin Film Photoanodes: A Time-Resolved Microwave Conductivity Study. *J. Phys. Chem. Lett.* **2013**, *4*, 2752–2757.

(49) Rettie, A. J. E.; Lee, H. C.; Marshall, L. G.; Lin, J. F.; Capan, C.; Lindemuth, J.; McCloy, J. S.; Zhou, J.; Bard, A. J.; Mullins, C. B. Combined Charge Carrier Transport and Photoelectrochemical Characterization of BiVO4 Single Crystals: Intrinsic Behavior of a Complex Metal Oxide. *J. Am. Chem. Soc.* **2013**, *135* (30), 11389–11396.

(50) Akiyama, S.; Nakabayashi, M.; Shibata, N.; Minegishi, T.; Asakura, Y.; Abdulla-Al-Mamun, M.; Hisatomi, T.; Nishiyama, H.; Katayama, M.; Yamada, T.; et al. Highly Efficient Water Oxidation Photoanode Made of Surface Modified LaTiO2N Particles. *Small* **2016**, *12* (39), 1–9.

(51) Chhajed, S.; Schubert, M. F.; Kim, J. K.; Schubert, E. F. Nanostructured Multilayer Graded-Index Antireflection Coating for Si Solar Cells with Broadband and Omnidirectional Characteristics. *Appl. Phys. Lett.* **2008**, *93* (25), 1–4.

(52) New Semiconductor Materials. Characteristics and Properties http://www.ioffe.rssi.ru/SVA/NSM/Semicond/ (accessed Jul 4, 2016).

(53) Puigdollers, A. R.; Schlexer, P.; Tosoni, S.; Pacchioni, G. Increasing Oxide Reducibility: The Role of Metal / Oxide Interfaces in the Formation of Oxygen Vacancies. *ACS Catal.* **2017**, No. 7, 6493−6513.

(54) Stein, H. S.; Soedarmadji, E.; Newhouse, P. F.; Dan Guevarra; Gregoire, J. M. Synthesis, Optical Imaging, and Absorption Spectroscopy Data for 179072 Metal Oxides. *Sci. data* **2019**, *6* (1), 9.

(55) Nandjou, F.; Haussener, S. Degradation in Photoelectrochemical Devices : Degradation in Photoelectrochemical Devices : Review with an Illustrative Case Study. *J. Phys. D. Appl. Phys.* **2017**, *50*, 1–23.

(56) Haussener, S. Computational tools https://lrese.epfl.ch/research/page-134145-en-html/ (accessed Jul 9, 2019).

(57) Gaudy, Y. K. POPe v.1. - Performance Optimization of Photoelectrode. EPFL 2019.
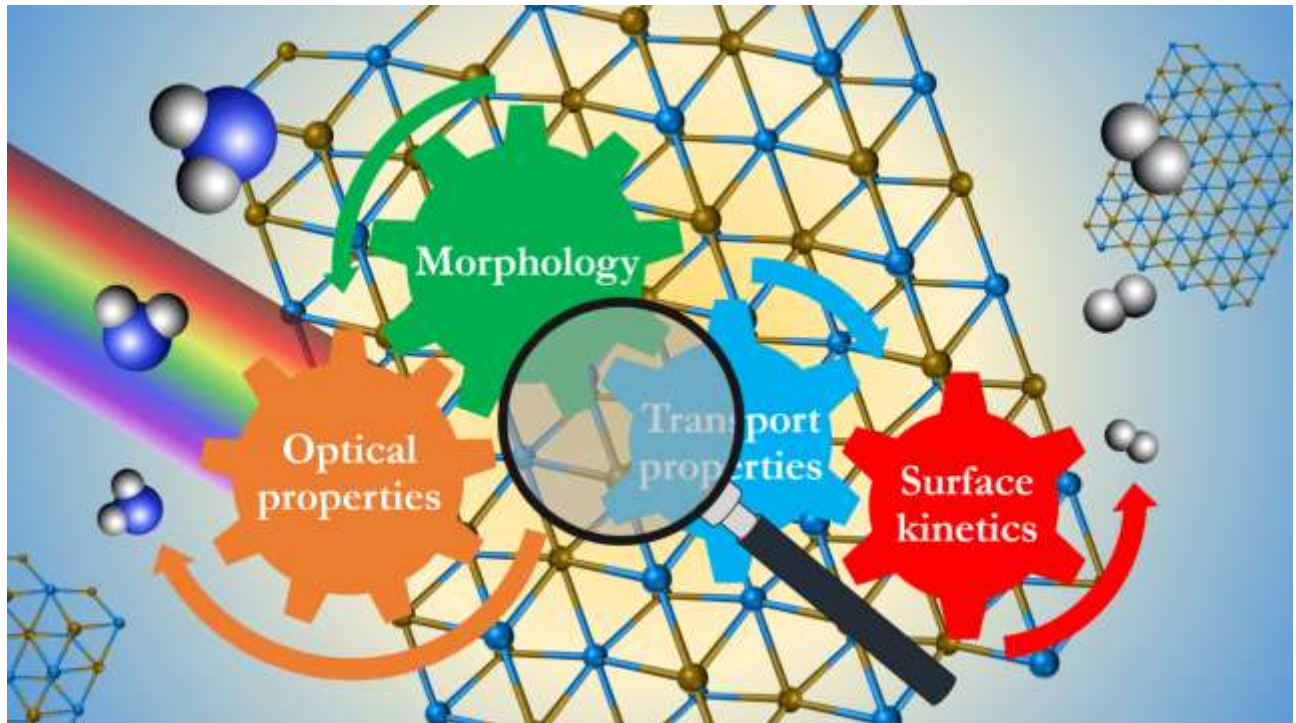
TOC figure (17x9.5 cm for conversion to 8.5x4.75 cm, 2008x1122 pixels)